HHS Public Access

Author manuscript

Nature. Author manuscript; available in PMC 2018 April 19.

Published in final edited form as:

Nature. 2017 October 19; 550(7676): 360–365. doi:10.1038/nature24060.

Promotion of RAD51-mediated homologous DNA pairing by BRCA1-BARD1

Weixing Zhao[1,*], **Justin B. Steinfeld**[2], **Fengshan Liang**[1,3,4], **Xiaoyong Chen**[3,4], **David G. Maranon**[5], **Chu Jian Ma**[2], **Youngho Kwon**[1], **Timsi Rao**[1], **Weibin Wang**[1], **Sheng Chen**[1,6], **Xuemei Song**[7], **Yanhong Deng**[7], **Judit Jimenez-Sainz**[8], **Lucy Lu**[1], **Ryan B. Jensen**[8], **Yong Xiong**[1], **Gary M. Kupfer**[3,4], **Claudia Wiese**[5], **Eric C. Greene**[2,*], and **Patrick Sung**[1,8,*]

[1]Department of Molecular Biophysics and Biochemistry, Yale University School of Medicine, New Haven, CT 06520, USA

[2]Department of Biochemistry & Molecular Biophysics, Columbia University, New York, NY 10032, USA

[3]Section of Hematology-Oncology, Department of Pediatrics, Yale University School of Medicine, New Haven, CT 06520, USA

[4]Department of Pathology, Yale University School of Medicine, New Haven, CT 06520, USA

[5]Department of Environmental and Radiological Health Sciences, Colorado State University, Fort Collins, CO 80523, USA

[7]Yale Center for Analytical Sciences, Yale School of Public Health, New Haven, CT, USA

[8]Department of Therapeutic Radiology, Yale University School of Medicine, New Haven, CT 06520, USA

Abstract

The tumor suppressor complex BRCA1-BARD1 functions in DNA double-strand break repair by homologous recombination. Therein, BRCA1-BARD1 facilitates the nucleolytic resection of DNA ends to generate a single-stranded template for the recruitment of another tumor suppressor complex BRCA2-PALB2 and the recombinase RAD51. By examining purified BRCA1-BARD1 and mutants, we show that BRCA1 and BARD1 both bind DNA and interact with RAD51, and

[*]Corresponding authors: weixing.zhao@yale.edu, ecg2108@cumc.columbia.edu and patrick.sung@yale.edu. Correspondence and requests for materials should be addressed to W.Z. (weixing.zhao@yale.edu), E.C.G (ecg2108@cumc.columbia.edu) or P.S. (patrick.sung@yale.edu).

[6]Present address: West China Hospital, Sichuan University, Chengdu, 610041, China

Supplementary Information
is linked to the online version of the paper at www.nature.com/nature.

Author Contributions
W.Z. and P.S. conceived the study. W.Z., E.C.G., G.M.K., C.W., and P.S designed the experiments and analyzed the data. W.Z., F.L., X.C., J.B.S., D.G.M., Y.K., C.S., T.R., W.W., C.S., L.L., and R.B.J generated key materials and executed the experiments. X.S. and Y.D. provided statistical analysis. W.Z. and P.S. wrote the paper with input from the other authors.

The authors declare no competing financial interests. Readers are welcome to comment on the online version of the paper

Data availability. The data that support the findings of this study are available from the corresponding author upon reasonable request.

that BRCA1-BARD1 enhances the recombinase activity of RAD51. Mechanistically, BRCA1-BARD1 promotes the assembly of the synaptic complex, an essential intermediate in RAD51-mediated DNA joint formation. Evidence is provided that BRCA1 and BARD1 are both indispensable for RAD51 stimulation. Importantly, BRCA1-BARD1 mutants weakened for RAD51 interaction are compromised for DNA joint formation and for the mediation of homologous recombination and DNA repair in cells. Our results identify a late role of BRCA1-BARD1 in homologous recombination, a novel attribute of the tumor suppressor complex that could be targeted in cancer therapy.

Mutations in *BRCA1* (breast cancer susceptibility gene 1) are linked to familial breast and ovarian cancers, and also to Fanconi anemia (FA)[1–5]. Following its discovery over twenty years ago[6–8], BRCA1 has been implicated in various biological processes including mRNA splicing and microRNA biogenesis[9–13], DNA damage signaling/cell cycle checkpoints[2,14], the avoidance of replication-transcription conflicts[15,16], and DNA doublestrand break (DSB) repair by homologous recombination (HR)[1,3,17–19]. The role of BRCA1 in these processes has remained mostly undefined, largely because of difficulties in obtaining high quality protein preparations for biochemical analyses. BRCA1 (1,863 residues) forms a stable complex with BARD1 (BRCA1-associated RING domain protein 1; 777 residues)[20,21]. Depletion of BARD1 engenders DNA damage sensitivity, HR deficiency, and genome destabilization[21–25]. The ablation of BARD1 in mice leads to cancer susceptibility[22], and probable disease causative mutations are found in cancer patients[26–30].

We strive to delineate the multifaceted role of BRCA1-BARD1 in HR-mediated DSB repair. During the repair process, the DSB ends are resected to yield 3′ single-stranded DNA tails[31]. These DNA tails become coated by Replication Protein A (RPA), which is subsequently displaced by the recombinase protein RAD51 to form a nucleoprotein complex termed the presynaptic filament. The presynaptic filament searches for, engages, and then invades a homologous duplex target to form a nascent heteroduplex DNA joint, the displacement loop or D-loop. This is followed by DNA synthesis and resolution of DNA intermediates to complete repair[32]. Published work has suggested that BRCA1 promotes DNA end resection by acting as an antagonist of 53BP1 and regulating the MRE11-RAD50-NBS1-CtIP complex, and also participates in RAD51 presynaptic filament formation with the tumor suppressors BRCA2 and PALB2[4,33]. To gain mechanistic insights into how BRCA1-BARD1 promotes HR, we have developed a robust system for co-expressing BRCA1 and BARD1 in insect cells and a protocol to obtain BRCA1-BARD1 for biochemical testing. Our results reveal novel attributes of BRCA1-BARD1 and a previously unrecognized role of this protein complex in the DNA strand invasion step of HR-mediated chromosome damage repair.

DNA binding by BRCA1 and BARD1

BRCA1-BARD1 was expressed in insect cells and purified to near homogeneity (Extended Data Fig. 1a–d). We employed the DNA electrophoretic mobility shift assay (EMSA) to test BRCA1-BARD1 for binding radiolabeled ssDNA, dsDNA, replication fork (RF), the D-loop, and DNA bubble. We also performed competition experiments in which the

nucleoprotein complex of BRCA1-BARD1 and radiolabeled D-loop was challenged with an unlabeled DNA species. The results revealed that BRCA1-BARD1 has the highest affinity for the D-loop and DNA bubble, followed by the RF, dsDNA, and ssDNA (Fig. 1a, b and Extended Data Figs. 1e–h; 2a,b).

BRCA1 is known to bind DNA[34,35]. Using the Southwestern assay, we found that both BRCA1 and BARD1 bind the D-loop, with BARD1 showing an apparently higher affinity for the substrate (Fig. 1c). Consistent with this, BRCA1-BARD1$^{1\text{-}142}$, which harbors full-length BRCA1 and only the RING domain of BARD1, exhibited a lower affinity for various DNA substrates (Extended Data Fig. 1i, j). Taken together, our results showed that both BRCA1 and BARD1 contribute to the DNA binding capability of the BRCA1-BARD1 complex. The DNA binding domain of BRCA1 was previously found to reside within the protein's middle region[34,35] and our mapping effort has led to the isolation of the BARD1 DNA binding domain (Extended Data Fig. 2c–e). Importantly, the BARD1 domain exhibited similar DNA binding properties as the complex (Extended Data Fig. 2f–i). Thus, BARD1 is a structure-specific DNA binding protein with the highest affinity for the D-loop and DNA bubble.

RAD51 interaction by BRCA1 and BARD1

BRCA1 was found to co-immunoprecipitate with RAD51 from cell extracts[17], but it has remained unclear whether it associates with RAD51 directly. By affinity pull-down, we found that BRCA1-BARD1 interacts with human RAD51 but has little or no affinity for yeast Rad51 (yRad51) (Fig. 1d) or *E. coli* RecA (Extended Data Fig. 3a). We also determined that 4–5 RAD51 molecules are bound by BRCA1-BARD1 (Extended Data Fig. 3b,c). Notably, formation of the BRCA1-BARD1-RAD51 complex was not affected by benzonase or ethidium bromide (Fig. 1d and Extended Data Fig. 3d), indicating that the association is not bridged by nucleic acid. Surprisingly, both BRCA1 and BARD1 retained RAD51 in the Far Western assay, with BARD1 showing a more robust signal (Fig. 1e), while the HR factors RAD51D-XRCC2 and DSS1 did not bind RAD51 under the same conditions (Extended Data Fig. 3e). These results helped establish that BRCA1-BARD1 associates with RAD51 in a species-specific manner, and that both proteins in the complex participate in RAD51 interaction.

Enhancement of homologous DNA pairing by BRCA1-BARD1

Given that BRCA1-BARD1 binds DNA and interacts with RAD51 (Fig. 1), we hypothesized that either it would enhance the assembly of the presynaptic filament and/or the potential of the presynaptic filament to mediate DNA strand invasion. We employed the DNA strand exchange assay[36,37] (Extended Data Fig. 4a) to test whether BRCA1-BARD1 would facilitate RAD51 presynaptic filament assembly. The results revealed that, while, as reported previously[36,38], the BRCA2-DSS1 complex promotes RAD51 presynaptic filament assembly on RPA-coated ssDNA, BRCA1-BARD1 does not possess such an attribute (Extended Data Fig. 4b, c). Moreover, we found that, unlike BRCA2-DSS1[37,38], BRCA1-BARD1 is devoid of the ability to target RAD51 to ssDNA when dsDNA is present (Extended Data Fig. 4d–f).

Next, the D-loop assay was conducted to test BRCA1-BARD1 for the promotion of DNA strand invasion (Fig. 2a). Importantly, BRCA1-BARD1, in amounts substoichiometric to RAD51, strongly enhanced the reaction, regardless of whether ATP (Extended Data Fig. 4g–i) or the non-hydrolyzable analogue AMP-PNP (Fig. 2a–c) was used as the nucleotide cofactor, while BRCA2-DSS1 did not show any stimulation (Fig. 2a–c). In contrast, BRCA1-BARD1 did not enhance the activity of yRad51 (Extended Data Fig. 4j, k). We found no stimulatory effect of BRCA2-DSS1 on D-loop formation by BRCA1-BARD1-RAD51 when the ssDNA substrate was pre-incubated with RAD51 or when ssDNA and plasmid DNA were premixed (Extended Data Fig. 5a, b). However, with RPA-coated ssDNA, D-loop formation became more robust with the combination of BRCA1-BARD1 and BRCA2-DSS1 than either complex alone (Extended Data Fig. 5c, d). Taken together, the results revealed an unexpected role of BRCA1-BARD1 in promoting DNA joint formation that is catalyzed by RAD51 (Fig. 2d).

In homologous DNA pairing, the presynaptic filament captures the duplex partner and then assembles the synaptic complex in which the recombining DNA molecules are aligned in homologous registry and base switching has occurred[32]. By monitoring the protection of dsDNA against restriction enzyme digestion (Fig. 3a), we found a stimulatory effect of BRCA1-BARD1 on synaptic complex formation (Fig. 3b, c). Next, we employed our DNA curtain assay[39,40] to examine the pairing of homologous DNA sequences in real time (Fig. 3d). As reported previously[39,40], the RAD51 presynaptic filament was able to engage a 70-bp dsDNA fragment harboring 9-nt homology (Fig. 3e). Importantly, the results showed an enhancement of DNA engagement by BRCA1-BARD1 (Fig. 3e). However, we found no evidence of BRCA1-BARD1 having any effect on the binding site distributions, the pairwise distance distributions, and the resident time (k_{off}) of the bound dsDNA (Fig. 3f, g and Extended Data Fig. 5e). Since BRCA1-BARD1 does not affect the k_{off} of the aligned dsDNA, we speculate that it acts by increasing the k_{on} of dsDNA engagement. We note that BRCA1-BARD1 mutants impaired for BARD1-RAD51 interaction or lacking the RAD51 interaction domain of BRCA1 are unable to promote pairing with the duplex target (see later). We also verified that BRCA1-BARD1 does not affect the ability of presynaptic filaments harboring yRad51 to engage dsDNA (Extended Data Fig. 5f and Fig. 3e).

Functional relevance of BARD1-RAD51 interaction

We sought to isolate RAD51-binding defective mutants of BRCA1-BARD1 for biochemical and genetic testing. First, we co-expressed RAD51 with various BRCA1 fragments in insect cells and conducted co-immunoprecipitation. Consistent with a previous study[17], $BRCA1^{1-1527}$ could interact with RAD51, while $BRCA1^{1-1000}$ and $BRCA1^{1-500}$ were impaired in this regard (Extended Data Fig. 6a–c). Importantly, BRCA1-BARD1 could co-precipitate much more RAD51 than BRCA1 alone. This result, together with the Far Western data (Fig. 1e), indicated that BARD1 harbors a major RAD51 interaction domain (Fig. 4a). Based on deletion analysis, the region between residues 123–162 of BARD1 was found to be indispensable for RAD51 interaction (Fig. 4a, b and Extended Data Fig.6d–g). Moreover, a GST-tagged BARD1 fragment harboring these residues could efficiently associate with RAD51 (Extended Data Fig. 6h), indicating that it encompasses the RAD51 interaction domain. We also discovered that the core domain of RAD51 (referred to as T3),

which has been implicated in BRCA2 binding via the BRC4 repeat of the latter[41], is able to interact with BRCA1-BARD1 (Extended Data Fig. 3f), but not with BRCA1-BARD1$^{1\text{-}142}$ or BRCA1$^{1\text{-}500}$-BARD1 (Extended Data Fig. 3g). Interestingly, we found that BRCA1-BARD1 can compete with BRCA2-DSS1 for RAD51 association (Extended Data Fig. 3h).

We expressed and purified the mutant BRCA1-BARD1$^{\Delta 123–162}$ complex that is deleted for the RAD51 interaction domain in BARD1. We found that BRCA1-BARD1$^{\Delta 123\text{-}162}$, while retaining normal DNA binding activity (Extended Data Fig. 7a, b), is defective in RAD51 interaction (Fig. 4c) and, accordingly, fails to enhance D-loop formation (Fig. 4d, e) or synaptic complex assembly (Extended Data Fig. 7c, d). Sequence alignment of the RAD51 interaction domain in BARD1 orthologs revealed a number of conserved amino acid residues (including the FXDA motif; Fig. 4b). Based on this information, we generated a compound mutant that changes the conserved residues F133 and D135 to alanine and A136 to glutamic acid (the AAE mutant); F133 was included as other RAD51 interaction motifs[41–43], such as BRC4 in BRCA2[41], also harbor a functionally indispensable F residue. We expressed and purified the mutant BRCA1-BARD1^{AAE} complex. Biochemical testing revealed that, even though the mutant complex binds DNA normally (Extended Data Fig. 7a, b), it is impaired not only for RAD51 association (Fig. 4c), but also for the ability to stimulate D-loop formation and synaptic complex assembly (Fig. 4d, e; Extended Data Figs. 5g and 7c, d). Together, these results provided evidence that the BRCA1-BARD1-RAD51 complex is indispensable for the enhancement of RAD51-mediated DNA strand invasion.

Cancer-associated mutations within the RAD51 interaction domain have been identified in BARD1, and one such mutation (K140N), found in two patients with colorectal adenocarcinoma or uterine corpus endometrial carcinoma, alters the conserved residue K140 (cBioPortal for Cancer Genomic)[44,45] next to the FXDA motif (Fig. 4b). To determine the significance of this mutation, the BRCA1-BARD1^{K140N} mutant complex was expressed and purified for testing. Importantly, the results revealed that, while the mutation has no impact on DNA binding (Extended Data Fig. 7a, b), it attenuates the affinity of BRCA1-BARD1 for RAD51 (Fig. 4c) and also compromises the ability of the tumor suppressor complex to enhance D-loop formation and synaptic complex assembly (Fig. 4d, e and Extended Data Fig. 7c, d).

Cellular role of the BRCA1-BARD1-RAD51 complex

Cell-based studies were conducted to examine the association between BRCA1-BARD1 and RAD51 and to ascertain the significance of the BRCA1-BARD1-RAD51 complex. We found that the amount of RAD51 co-immunoprecipitating with BARD1^{WT}*res* is enhanced by MMC treatment of cells (Fig. 5a) and, importantly, that the BARD1^{AAE}*res* mutation impairs the DNA damage-induced association with RAD51 (Fig. 5a). Cellular fractionation confirmed that the nuclear localization of BRCA1 and BARD1 is not affected by the BARD1^{AAE}*res* mutation (Extended Data Fig. 8a).

Next, we employed the DR-GFP reporter[46,47] and the CRISPR/Cas9-stimulated gene targeting assay[48,49] to ask whether the BARD1^{AAE}*res* mutation affects HR proficiency. As expected, knockdown of endogenous BRCA1 or BARD1 by siRNA impaired HR in both

systems (Extended Data Fig. 8b–d). Importantly, while the ectopic expression of BARD1^{WT}*res* in BARD1 deficient cells fully restored HR proficiency, that of BARD1^{AAE}*res* resulted in only partial complementation (Fig. 5b, c and Extended Data Fig. 9a, b). Moreover, in clonogenic cell survival assays, BARD1 deficient cells that harbored BARD1^{AAE}*res* were markedly more sensitive to MMC and to the PARP inhibitor Olaparib than cells expressing BARD1^{WT}*res* (Fig. 5d and Extended Data Fig. 9c).

We also investigated whether the BARD1^{AAE}*res* mutation would affect the DNA damage-induced assembly of RAD51 nuclear foci. As expected, knockdown of endogenous BRCA1 diminished RAD51 focus formation, either spontaneously or after γ-ray exposure (Extended Data Fig. 8e–g). Interestingly, treatment with BARD1 siRNA impaired RAD51 focus formation to a lesser extent (Extended Data Fig. 8g). In cells depleted of endogenous BARD1 and expressing BARD1^{WT}*res* or BARD1^{AAE}*res*, RAD51 focus formation occurred similarly, both spontaneously and after γ-irradiation (Extended Data Fig. 9d, e). However, as indicated by S4/S8 phosphorylation of RPA32, BARD1^{AAE}*res* cells retained a much higher level of DNA damage 72 h after release from MMC treatment (Extended Data Fig. 9f). These results showed that HR repair is deficient in BARD1^{AAE}*res* cells even though RAD51 focus formation is not affected. Interestingly, even though depletion of 53BP1, an inhibitor of DNA end resection[50], partially overcame the HR defect associated with BRCA1 deficiency (Extended Data Fig. 8h, i), it did not suppress the HR defect in BARD1 deficient cells (Extended Data Fig. 8j, k). In cells lacking both BARD1 and 53BP1, BARD1^{AAE}*res* was less capable than BARD1^{WT}*res* in complementing the HR deficiency (Extended Data Fig. 8l, m). Taken together, our results helped establish the biological significance of the BRCA1-BARD1-RAD51 complex in DNA damage repair via HR and provide cellular evidence for a role of BRCA1-BARD1 in the DNA strand invasion step of HR.

Role of BRCA1 in RAD51-mediated homologous DNA pairing

For interrogating the role of BRCA1 in RAD51-mediated reactions, we expressed and purified BRCA1$^{1\text{-}500}$-BARD1, which lacks the RAD51 interaction and DNA binding domains of BRCA1[17,34], and also BRCA1$^{\Delta 758\text{-}1064}$-BARD1, which is deleted for the RAD51 interaction domain of BRCA1. These mutant complexes appeared to be proficient in DNA binding (Extended Data Fig. 10a–e) but were weakened for RAD51 interaction (Extended Data Fig. 10f–h). Importantly, neither mutant complex could strongly enhance RAD51-mediated D-loop formation (Extended Data Fig. 10i, j) or synaptic complex assembly (Extended Data Figs. 5g and 7c–f). Thus, BRCA1 is also indispensable for the functional integrity of BRCA1-BARD1 as a co-factor of RAD51.

Discussion

Our study has revealed a novel role of BRCA1-BARD1 in the enhancement of DNA invasion in HR via a direct interaction with RAD51 (Fig. 6). Mechanistically, BRCA1-BARD1 functions with the RAD51 presynaptic filament in the assembly of the synaptic complex, a critical precursor to D-loop formation (Fig. 6). Both BRCA1 and BARD1 are indispensable for this attribute. It is likely that physical association with RAD51 facilitates dsDNA engagement by the presynaptic filament and that the specific recognition of

unwound DNA by BRCA1-BARD1 enhances the formation of the nascent DNA joint in the D-loop reaction. Since we have not observed significant stimulation by BRCA1-BARD1 of DNA strand exchange between an oligonucleotide and a short linear duplex, it remains possible that the complex facilitates DNA homology search within a long duplex DNA target. A model incorporating this new function and the known roles of BRCA1-BARD1 in DNA end resection and RAD51 presynaptic filament assembly is shown in Figure 6.

The findings from our study open up a new avenue towards understanding how mutations in BRCA1-BARD1 affect its DNA damage repair and tumor suppression functions. Indeed, we have provided evidence that the cancer-associated mutation K140N in BARD1 compromises the physical and functional interactions of BRCA1-BARD1 with RAD51. We note that the region of BRCA1 (amino acid residues 758-1064) that harbors the RAD51 interaction domain[17] is frequently mutated in cancer (cBioPortal for Cancer Genomic)[44,45] and that deletion of this domain abolishes the activity of BRCA1-BARD1 in RAD51-mediated DNA strand invasion (this study). The biochemical systems established in our work should be valuable for determining the impact of pathogenic mutations on BRCA1-BARD1 functions. Moreover, our findings may guide the development of targeted therapy of breast, ovarian, and other cancers.

Methods

Construction of plasmids

A His_6 affinity tag was fused to BARD1 in pFastbac-BARD1 (from Jeffrey Parvin) using the QuikChange mutagenesis kit (Stratagene). The mammalian pS-Flag-SBP-BARD1*res* expression vector was modified by removing the GFP coding sequence from the pS-Flag-SBP-BARD1 vector (from Xiaochun Yu) and introducing silent mutations into the siRNA target regions of BARD1 using oligos 1 & 2 and oligos 3 & 4, respectively (see Extended Data Table 1). QuikChange site-directed mutagenesis was used to construct the mutant forms of BARD1, namely, $BARD1^{1\text{-}122}$, $BARD1^{1\text{-}162}$, $BARD1^{1\text{-}261}$, $BARD1^{\Delta 123\text{-}162}$, $BARD1^{\Delta 123\text{-}261}$, $BARD1^{\Delta 163\text{-}261}$, $BARD1^{AAE}$ and $BARD1^{K140N}$ (The sequences of the primers used are available upon request). $BARD1^{123\text{-}162}$ was introduced into pDEST15 for expression of the GST-tagged form of this BARD1 fragment in *E. coli.* $BARD1^{124\text{-}270}$ was cloned into pE-SUMO vector (LifeSensors Inc.) for expression of the SUMO-tagged form of this BARD1 domain in *E. coli.*

Protein purification

Purification of BRCA1-BARD1 from insect cells—pFastbac-Flag-BRCA1 (from Jeffrey Parvin) and pFastbac-His-BARD1 were introduced into *E. coli* strain DH10Bac for bacmid generation. The bacmids were used to transfect SF9 insect cells to generate recombinant baculoviruses. After amplification in SF9 cells, the viruses were used to infect Hi5 insect cells for expression of BRCA1 and BARD1 (10 ml BRCA1 and 10 ml BARD1 P3 viruses for 600 ml culture). After a 44-h incubation at 27°C, cells were harvested by centrifugation, frozen in liquid nitrogen, and stored at −80°C. All purification steps were carried out at 0°C to 4°C. To prepare extract, the frozen cell pellet (8 g, from 600 ml culture) was thawed and suspended in 40 ml of cell breakage buffer A (50 mM Tris-HCl, pH 7.5, 500

mM KCl, 1 mM 2-mercaptoethanol, 0.5% NP-40, 5 mM $MgCl_2$, 2 mM ATP and the following protease inhibitors: aprotinin, chymostatin, leupeptin, and pepstatin A at 3 μg/ml each, and 1 mM PMSF) for cell lysis using a Dounce homogenizer type B pestle (30 strokes). The lysate was cleared by centrifugation at 10,000 × g for 15 min, and the supernatant was incubated with 3 ml anti-Flag M2 affinity resin (Sigma) for 2 h. The resin was transferred to a column (1.5 × 15 cm), washed with 50 ml lysis buffer and then with 50 ml buffer B (25 mM Tris-HCl, pH 7.5, 300 mM KCl, 10% glycerol, 0.5 mM EDTA, 0.01% Igepal CA-630, 1 mM 2-mercaptoethanol, 5 mM $MgCl_2$ and 2 mM ATP), before the bound proteins were eluted four times with 2 ml of buffer B containing the single Flag peptide (200 μg/ml). The eluates were combined and mixed with 32 ml buffer C (25 mM Tris-HCl, pH 7.5, 10% glycerol, 0.5 mM EDTA, 0.01% Igepal CA-630, 1 mM 2-mercaptoethanol) before being further fractionated in a 1 ml HiTrap SP Sepharose HP column (GE Healthcare) using a 12 ml gradient of 75–500 mM KCl in buffer C. The pooled BRCA1-BARD1 fractions (from 250–350 mM KCl) were further fractionated in a gel filtration column of Superose 6 10/300 GL (GE Healthcare), which was developed with 24 ml of buffer C containing 300 mM KCl. The peak fractions were pooled, divided into 10 μl portions, frozen in liquid nitrogen, and stored at −80°C. The mutant forms of BRCA1-BARD1 were expressed and purified using the same procedures. The yield of highly purified BRCA1-BARD1 from 600 ml insect cell culture ranged from 150 to 300 μg with a final concentration of 300 to 500 μg /ml.

Purification of BARD1$^{123\text{-}162}$ andBARD1$^{124\text{-}270}$ from E. coli—The GST-BARD1$^{123\text{-}162}$ expression plasmid pDEST15-BARD1$^{123\text{-}162}$ or the BARD1$^{124\text{-}270}$ expression plasmid pET-SUMO-BARD1$^{124\text{-}270}$ was introduced into *E. coli* Rosetta (DE3) cells. An overnight culture derived from a single colony in 50 ml LB medium grown at 37°C was used to inoculate 2 L fresh LB medium. IPTG was added to 0.4 mM when the cell density had reached OD_{600}=0.8, and cells were harvested after a 16-h incubation at 16°C. All the subsequent steps were carried out at 0–4°C. The cell pellet (8 g) was suspended in 50 ml buffer D (20 mM KH_2PO_4, pH 7.5, 10% glycerol, 0.5 mM EDTA, 0.01% Igepal CA-630, 1 mM 2-mercaptoethanol and 300 mM KCl) containing the protease inhibitors (aprotinin, chymostatin, leupeptin, and pepstatin A at 3 μg/ml each, and 1 mM PMSF) and cell lysate was prepared by sonication. After centrifugation (100,000 × g for 90 min), the clarified lysate was incubated with 2 ml Glutathione Sepharose 4 Fast Flow resin (GE Healthcare; for GST-BARD1$^{123\text{-}162}$) or Ni-NTA resin (GE healthcare; for BARD1$^{124\text{-}270}$) for 2 h. The affinity resin was transferred to a glass column (1.5 × 15 cm), washed with 20 ml buffer D, before being eluted 3 times with 3 ml of 20 mM glutathione or 150 mM imidazole in buffer D. For BARD1$^{124\text{-}270}$, the His_6-SUMO tag was cleaved by the Ulp1 protease by an overnight incubation at 4°C. The eluates were pooled and concentrated in a Centricon-10K concentrator (Amicon) to 0.5 ml before being further fractionated in a Superdex 200 10/300 GL column (GE Healthcare) with 24 ml of buffer C containing 300 mM KCl. The peak fractions were pooled, concentrated to ~100 μl as above, divided into 5 μl portions, frozen in liquid nitrogen, and stored at −80°C.

Other recombination proteins—BRCA2-DSS1, RAD51, RPA and yeast Rad51 were purified to near homogeneity using our previously described procedures[36,51,52].

DNA substrates and DNA binding assay

D-loop, DNA bubble, replication fork and double-stranded DNA were assembled from oligonucleotides 5/6/7, oligonucleotides 5/6, oligonucleotides 8/9/10/11 and oligonucleotides 12/13, respectively (see Extended Data Table 1 for oligonucleotide sequences); the asterisk identifies the oligonucleotide that was ^{32}P-labeled at its 5′ end in each substrate. The single-stranded DNA substrate was 5′ ^{32}P-labeled oligonucleotide 12. These DNA substrates (10 nM each) were incubated with wild type or the specified mutant form of BRCA1-BARD1 at 37°C in 10 μl buffer E (25 mM Tris-HCl, pH 7.5, 90 mM KCl, 1 mM DTT, and 100 μg/ml bovine serum albumin (BSA)) for 10 min. After the addition of loading buffer (50% glycerol, 20 mM Tris-HCl, pH 7.4, 0.5 mM EDTA, 0.05% Orange G), the reaction mixtures were resolved by 6% native polyacrylamide gel electrophoresis in TAE buffer (30 mM Tris-acetate, pH 7.4 and 0.5 mM EDTA) at 4°C. The gels were dried, and DNA species were visualized by autoradiography and quantified using the Personal Molecular Imager™ and Quantity One software (Bio-Rad). Since the nucleoprotein complexes formed by BRCA1-BARD1 do not always migrate as well-defined species, we quantified DNA binding by measuring the disappearance of the DNA substrate.

Affinity pulldown

RAD51, yRad51 or RecA (5 μM) was incubated with 0.5 μM of Flag-BRCA1-BARD1 or 3 μM of GST-BARD1$^{123\text{-}162}$ at 4°C for 30 min in 30 μl buffer F (25 mM Tris-HCl pH 7.5, 10% Glycerol, 0.5 mM EDTA, 0.05% Igepal CA-630, 1 mM 2-mercaptoethanol, 150 mM KCl). Then, the reaction mixture was mixed with 12 μl anti-Flag M2 affinity resin or Glutathione Sepharose 4 Fast Flow resin at 4°C for 30 min to capture protein complexes through the Flag tag on BRCA1 or the GST tag on BARD1, respectively. After washing the resin three times with 200 μl buffer F, bound proteins were eluted with 20 μl 2% SDS at 37°C for 5 min. The supernatant (S), last wash (W) and SDS eluate (E), 8 μl each, were analyzed by SDS-PAGE and Coomassie blue staining.

Southwestern analysis

BRCA1-BARD1 was resolved in a 7.5% SDS-PAGE gel and transferred onto a nitrocellulose membrane (Bio-Rad) at 4°C in transfer buffer (25 mM Tris-HCl, 192 mM glycine, pH 8.3, 20% methanol). After being soaked in buffer G (25 mM Tris-HCl, pH 7.5, 2 mg/ml BSA, 1 mM DTT, 0.1% Triton X-100, 10% glycerol and 100 mM KCl) at 4°C for 20 h, the membrane was rinsed twice with buffer H (25 mM Tris-HCl, pH 7.5, 200 μg/ml BSA, 90 mM KCl, 4 mM $MgCl_2$ and 1 mM DTT) and then incubated in 10 ml buffer H containing ^{32}P-labeled D-loop DNA (2 nM) at 25°C for 1 h. The membrane was washed four times with 10 ml buffer H before analysis by phosphorimaging.

Far Western analysis

After SDS-PAGE, BRCA1 and BARD1 were transferred onto a nitrocellulose membrane, as described for the Southwestern analysis. The membrane was soaked in buffer I (10 mM KH_2PO_4 at pH 7.4, 150 mM KCl, 15 mg/ml BSA, 2 mM 2-mercaptoethanol, 0.05% Tween 20) at 25°C for 2 h and then incubated with 5 μg/ml RAD51 in buffer I at 25°C for 2 h. Then, the membrane was washed with 10 ml buffer I three times, incubated with anti-

RAD51-HRP antibodies (Abcam, ab195548) for 1 h in buffer I, washed again with 10 ml buffer I three times, and developed with the Super Signal Substrate Kit (Pierce).

Homologous DNA pairing assay

This was conducted as described[36,37]. The reaction was assembled in buffer J (25 mM Tris-HCl, pH 7.5, 60 mM KCl, 1 mM DTT and 100 μg/ml BSA) containing 1 mM ATP and 2 mM $MgCl_2$ in a final volume of 12.5 μl. For mediator activity, the 150-mer oligonucleotide 14 (6 μM nucleotides) was first incubated with RPA (600 nM) at 37°C for 5 min, and then RAD51 (2 μM) with or without the indicated concentration of BRCA1-BARD1 or BRCA2-DSS1 was incorporated into the reaction. Following a 5-min incubation at 37°C, ^{32}P-labeled homologous dsDNA (40 bp; oligos 15 & 16; 1.6 μM base pairs) and 4 mM spermidine hydrochloride were added. For testing of ssDNA targeting activity, RAD51 was incubated with the mixture of ssDNA, ^{32}P-labeled dsDNA and spermidine hydrochloride with and without BRCA1-BARD1 or BRCA2-DSS1 for 30 min. The reaction was terminated by adding an equal volume of 1% SDS containing 1 mg/ml proteinase K. Following a 5-min incubation at 37°C, the deproteinized reaction mixtures were resolved in an 8% non-denaturing polyacrylamide gel in TAE buffer. The gel was dried onto 3MM CHR cellulose chromatography papers (GE Healthcare), and DNA species were visualized by autoradiography and quantified, as above.

D-loop assay

This was conducted as described[42,53]. Briefly, the ^{32}P-labeled 90-mer oligonucleotide 17 (2.4 μM nucleotides) was incubated with RAD51 (1 μM) at 37°C for 5 min in buffer J containing 1 mM $MgCl_2$ and 2 mM ATP or AMP-PNP. Following the incorporation of the indicated concentration of BRCA1-BARD1 and a 5-min incubation at 37°C, the Dloop reaction was initiated by adding pBluescript SK replicative form I DNA (37 μM base pairs) and was incubated at 37°C for 7 min. The molar ratio of the 90-mer to pBluescript plasmid in the reactions was 2.1 to 1. The reaction was terminated by adding an equal volume of 1% SDS containing 1 mg/ml proteinase K and a 5-min incubation at 37°C. The deproteinized reaction mixtures were resolved by electrophoresis in a 1% agarose gel, which was dried onto Hybond™ -N membrane (GE Healthcare). Phosphorimaging analysis was used to visualize and quantify the radiolabeled DNA species.

Synaptic complex assay

The assay was conducted at 37°C as described[5,6]. Briefly, RAD51 (4 μM) was incubated with the 60-mer oligonucleotide 18 (12 μM nucleotide), which is homologous to the *Ssp*I restriction site in the target pUC19 dsDNA, in 8 μl of buffer K (35 mM Tris-HCl, pH 7.5, 50 mM KCl, 2 mM ATP, 2 mM $MgCl_2$, 100 μg/ml BSA, and 1 mM DTT) for 5 min. After adding the indicated amounts of BRCA1-BARD1 in 1 μl volume, the reaction mixture was incubated for 5 min. Then, linear pUC19 plasmid DNA (85 μM nucleotides) was added in 1 μl, followed by a 5-min incubation and the treatment with 2.5 units of *Ssp*I for 10 min. The reaction mixtures were resolved by agarose gel electrophoresis in TAE buffer, and DNA species were stained with ethidium bromide. The heterologous oligonucleotide 19 (Extended Data Table 1) was used as a control.

DNA curtain imaging analysis

RAD51 filaments were assembled on ssDNA curtains, and the dsDNA-binding properties of the resulting RAD51-ssDNA filaments were measured as described[39,40]. To determine the number of dsDNA-binding events, BRCA1-BARD1 was diluted from a 1.5 μM stock with Buffer K (30 mM Tris–acetate pH 7.5, 1 mM $MgCl_2$, 5 mM $CaCl_2$, 100 mM KCl, 2 mM ATP, 1 mM DTT, and 0.2 mg/ml BSA) to concentrations ranging from 10–100 nM, introduced into the flow cell chamber, followed by a 10-min incubation at 37°C. After washing with 1 ml of Buffer K (at 1 ml/min), 2.16 nM Atto565-labeled dsDNA (70-bp) with 9-nt of homology (oligos 20 & 21) to the RAD51-ssDNA filaments was introduced into the chamber, followed by a 10-min incubation at 37°C. Then, the cell was washed with 0.5 ml buffer K (at 1 ml/min) and three images were taken. The length of each of the RAD51-ssDNA filaments and number of labeled-dsDNA molecules bound were recorded and normalized to a length of 50 pixels (~40kb). Weighted average and standard deviation based on the length of each filament were calculated. Confidence intervals of 95% are represented as error bars. For survival probabilities, experiments were conducted without or with 100 nM BRCA1-BARD1 and 100 ms exposures were recorded every 30 seconds over 90 min. Dwell times of ~180 molecules were determined for each experiment by kymograph and survival probabilities were plotted on a semi-log plot. Error bars represent 70% confidence as measured by bootstrap analysis, a close approximation of one standard deviation from the mean.

Cell culture and transfection

U2OS and HeLa cells from ATCC were grown in Dulbecco's modified Eagles medium (DMEM) supplemented with 10% fetal bovine serum (Sigma), 100 μg/ml streptomycin, and 100 U/ml penicillin (Sigma). The cells were tested for mycoplasma contamination by Bionique testing labs (http://www.bionique.com/). Qiagen siRNA oligonucleotides used to transiently deplete BARD1 and BRCA1 are listed in Extended Data Table 1. 53BP1 siRNA (s14313) was purchased from Ambion-Thermo Fisher Scientific. Transfection of siRNA, pS-Flag-SBP-BARD1*res* and pCMV-I-SceI-3xNLS was carried out using Lipofectamine 2000 (Invitrogen) according to the manufacturer's instructions. To generate stable HeLa and U2OS cell lines expressing Flag-SBP-BARD1 or its mutants, cells were transfected with their respective plasmids (pS-Flag-SBP-BARD1^{WT}*res*, pSFlag-SBP-BARD1^{AAE}*res,* and pS-Flag-SBP-BARD1^{K140N}*res*) and individual clones were selected with 800 μg/ml G418.

Co-immunoprecipitation analysis

HeLa cells grown on 15 cm cell culture dishes were treated with or without 1 μM MMC overnight prior to harvest. Following a wash with PBS (phosphate buffered saline), cells were scraped off and transferred to Eppendorf tubes. Whole cell lysate was prepared by adding 1 ml of lysis buffer (300 mM NaCl, 1.0% Triton X-100, 5 mM EDTA, 2 mM $NaVO_4$, 2 mM $Na_4O_7P_2$, 0.02% NaN_3, and 50 mM Tris-HCl, pH7.4) with protease inhibitors (Roche Complete Protease Inhibitor Cocktail Tablet) to cell pellets. Following a 12-s sonication, the cell extract was cleared by centrifugation at 18,400g for 15 min at 4°C. The supernatant fraction (2 mg protein in total) was incubated with DNase I (20U) for 15 min at room temperature and 15 min at 37°C. Then, 50 μl of anti-Flag resin (Sigma) or anti-mouse IgG

resin (Santa Cruz) was added, followed by a 12 h incubation at 4°C overnight. After washing the resin 4 times with lysis buffer, bound proteins were eluted with 100 μl SDS gel loading buffer (50 mM Tris-HCl pH 6.8, 2% SDS, 0.1% bromophenol blue, 10% glycerol, 10% 2-mercaptoethanol) and 100 μl of the eluates were subject to Western blot analysis with anti-Flag and anti-RAD51 antibodies.

Immunoblot analysis

Protein was extracted from cells harvested two days after transfection with the indicated siRNAs using NETN buffer (20 mM Tris-HCl pH 8, 420 mM NaCl, 1 mM EDTA, 0.5% Igepal CA-630, 1 mM DTT, and Roche Protease Inhibitor Cocktail) and 8 freeze/thaw cycles. Blots (20–50 μg of total protein) were probed with the following antibodies: BARD1 (Bethyl, A300-263A; Santa Cruz Biotech, Sc11438), BRCA1 (Abcam, ab16780), 53BP1 (Abcam, ab36823), Flag M2-HRP (Sigma, A8592), Phospho RPA32 S4/S8 (Bethyl, A300-245A), BRCA2 (EMD Millipore, OP95-100UG), RAD51 (Santa Cruz Biotech, sc-8349), Actin (Abcam, ab3280), Tubulin (Santa Cruz Biotech, sc-53030), HA.11 (16B12) (Covance, MMS-101P), or GST-HRP (NEB, E2624S) according to the instructions provided by the manufacturers. If needed, the blots were incubated with HRP-conjugated secondary antibodies (Pierce 31450 for rabbit anti-mouse IgG-HRP; Sigma A6154 for goat anti-rabbit IgG-HRP; Santa Cruz Biotech Sc-2032 for goat anti-rat IgG-HRP) before visualization of protein signals using the ECL kit (Thermo Scientific Pierce).

DR-GFP reporter assay

The DR-U2OS cell line containing a single integrated copy of the DR-GFP reporter was used[46,47]. Exponentially growing cells were seeded in 6-well plates at 2×10^5 cells per well prior to transfection with 2 μl siRNA (20 μM) and 5 μl Lipofectamine™ 2000 (Invitrogen). One day after siRNA transfection, cells were transfected with 2 μg I-*Sce*I expression vector (pCBASce) and 5 μl Lipofectamine™ 2000. HR proficiency was determined by counting the fraction of GFP-positive cells using a BD FACS Calibur S at 72 h post I-*Sce*I transfection. The results were derived from 3 to 5 transfections of at least 3 independent experiments.

CRISPR/Cas9-induced gene targeting assay

The assay was conducted as described[48]. U2OS cells were seeded in 6-well plates at 2×10^5 cells prior to transfection with 2 μl siRNA (20 μM) and 5 μl Lipofectamine™ 2000 (Invitrogen). One day after siRNA transfection, cells were co-transfected with 1.6 μg sgRNA plasmid pX330-LMNA1 (from Graham Dellaire) and 0.4 μg donor template pCR2.1-CloverLamin (from Graham Dellaire) and 5 μl Lipofectamine™ 2000 (Invitrogen). Gene targeting efficiency was determined by counting the percent of Clover-positive cells using a BD FACS Calibur S at 72 h post plasmids co-transfection. The results were derived from 3 to 5 transfections of at least 3 independent experiments.

Immunofluorescence microscopy and image analysis

HeLa Cells in exponential growth were transfected on two consecutive days in Opti-MEM medium using RNAiMAX (Invitrogen) with 20 nM BARD1 or control siRNA, as recommended by the manufacturer. Exposure to γ-ray was performed using a ^{137}Cs γ-

irradiator (J.L. Shepherd, model 81-14) and a dose rate of 1.05 Gy/min. Immunohistochemistry was performed as previously described[54], except that cells were fixed in 4% paraformaldehyde at room temperature for 10 min and permeabilized in 0.4% Triton X-100 in PBS for 5 min. Rabbit anti-RAD51 (H-92; Santa Cruz Biotechnology; 1:2000) and goat anti-rabbit AlexaFluor-488 secondary antibodies (Invitrogen; 1:750) were used. For image capture of RAD51 foci, Z-stack section images consisting of 20 stacks (0.2 μm intervals) from 100–150 nuclei per sample were taken using a 63×oil objective and a Zeiss Axio-Imager.Z2 microscope equipped with Zen Blue software (Carl Zeiss Microscopy, LLC, Thornwood, NY). For computational analyses of foci, Z-stacks were collapsed down to the maximum intensity projections, and a combination of ImageJ (http://rsb.info.nih.gov/ij/) and Cell Profiler (http://www.cellprofiler.org/) software programs was used with the following custom program settings for image processing: minimum object size=3; maximum object size=35; despeckle ratio=0.3; rolling ball size=5. A custom-built pipeline for automated cell (80–300 pixel units) and foci counting with settings for shape (i.e. 0.5) and dimensions (i.e. 5 pixels diameter) was employed. The threshold for foci detection was determined based on sham-irradiated samples, and nuclei with >5 foci/nucleus were counted positive. Group allocation and outcome assessment were done in a fully blinded manner.

Clonogenic survival assay

HeLa cells were transiently transfected with siRNA as described above. After 48 hours, cells were seeded into 6-well plates at 50–32,000 cells/well, treated with 0, 5, 10 and 20 nM MMC (Sigma) or 0, 0.5, 1 and 2 μM Olaparib (Selleckchem) in regular growth medium for 14 days. Cells were fixed with 10% methanol and 10% acetic acid, and stained with 1% crystal violet in methanol before colonies were counted. Clonogenic survival was determined for a given concentration of cells that were plated by dividing the number of colonies on each treated plate by the number of colonies on the untreated plate, taking the plating efficiency of untreated cells into account.

Preparation of cytoplasmic and nuclear extracts

The Dignam method for the preparation of cytoplasmic and nuclear extracts was followed[55]. Briefly, 10^9 cells were washed with PBS and Dignam buffer A (10 mM Hepes pH 7.9, 1.5 mM $MgCl_2$, 10 mM KCl, 0.5 mM DTT and 0.5 mM PMSF), collected by centrifugation, and lyzed in 2 packed cell volumes of Dignam buffer A using a Dounce homogenizer (50 strokes) with the type A pestle. After centrifugation, the supernatant containing cytoplasmic proteins was saved for analysis. The pelleted nuclei were resuspended and lysed in 3 ml Dignam buffer C (20 mM Hepes pH 7.9, 1.5 mM $MgCl_2$, 420 mM NaCl, 0.2 mM EDTA, 0.5 mM DTT, 25% glycerol, and 0.5 mM PMSF) using a Dounce homogenizer (80 strokes) with the type B pestle. Debris was removed by centrifugation to yield the nuclear extract fraction. The cytoplasmic and nuclear fractions, 20 μg each, were analyzed by immunoblotting for their content of BRCA1, Flag-SBPBARD1, Tubulin and Histone H3.

Statistics and Reproducibility

The statistical analysis was performed using Prism 7 (GraphPad Software, Inc., La Jolla, CA; http://www.graphpad.com/quickcalcs/ttest1.cfm) on the data from at least three independent experiments, as specified. Unless stated otherwise, statistical significance was

assessed by two-tailed unpaired Student's t-test. P ≤0.05 (*) and P ≤0.01 (**) was considered significant.

Extended Data

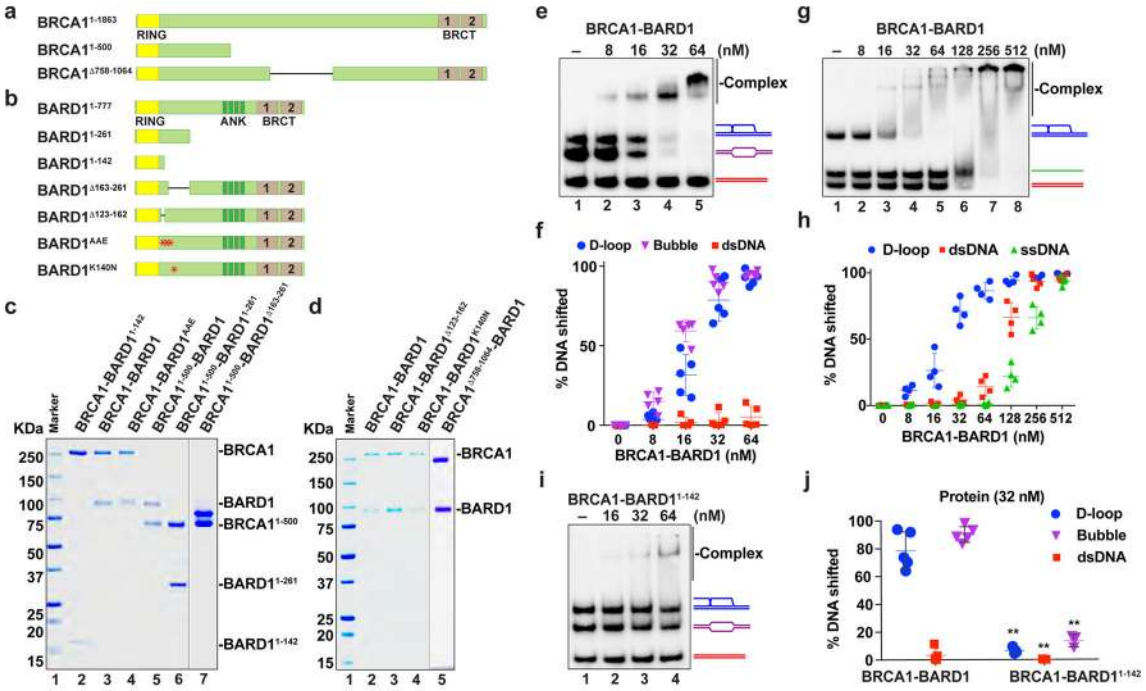

Extended Data Fig. 1. Purification of BRCA1-BARD1 and mutant variants, and DNA binding properties of BRCA1-BARD1 and BRCA1-BARD1$^{1-142}$

a–b, Schematic of BRCA1 (**a**) and BARD1 (**b**) and mutant variants of these proteins tested in this study. **c**, SDS-PAGE of purified BRCA1-BARD1$^{1-142}$ (lane 2), BRCA1-BARD1 (lane 3), BRCA1-BARD1^{AAE} (lane 4), BRCA1$^{1-500}$-BARD1 (lane 5), BRCA1$^{1-500}$-BARD1$^{1-261}$ (lane 6) and BRCA1$^{1-500}$-BARD1$^{Δ163-261}$ (lane 7). Size markers were run in lane 1. **d**, SDS-PAGE of purified BRCA1-BARD1 (lane 2), BRCA1-BARD1$^{Δ123-162}$ (lane 3), BRCA1-BARD1^{K140N} (lane 4) and BRCA1$^{Δ758-1064}$-BARD1 (lane 5). Size markers were run in lane 1. **e,** DNA binding test of BRCA1-BARD1 with the mixture of D-loop, DNA bubble and dsDNA. **f**, Quantification of **e**. Data are means ± s.d., n=5. **g**, DNA binding test of BRCA1-BARD1 with the mixture of D-loop, dsDNA and ssDNA. **h**, Quantification of **g**. Data are means ± s.d., n=4. **i**, DNA binding test of BRCA1-BARD1$^{1-142}$ with the mixture of D-loop, DNA bubble and dsDNA. **j**, Quantification of the results obtained with 32 nM of protein complexes in **e** and **i**. Data are means ± s.d., n=3 or 5. **, P<0.01.

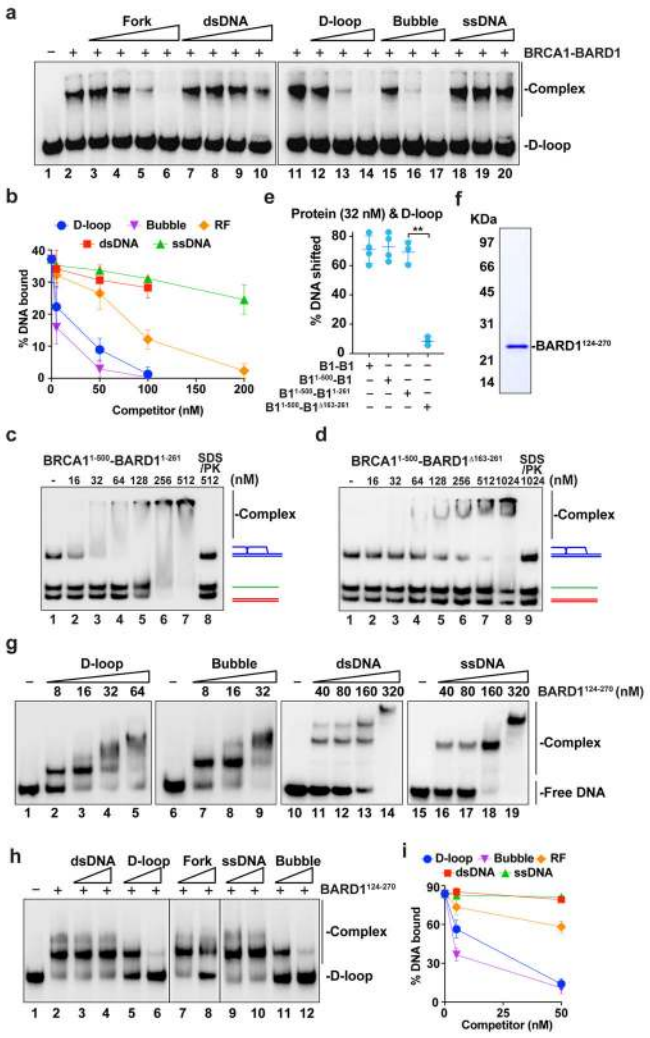

Extended Data Fig. 2. DNA binding by BARD1

a, BRCA1-BARD1 (5 nM) was incubated with radiolabeled D-loop (10 nM) and then the nucleoprotein complex was presented with an increasing concentration of unlabeled ssDNA, dsDNA, fork, bubble or D-loop as indicated. **b,** Quantification of **a**. Data are means ± s.d., n=2 or 3. **c,** DNA binding test of BRCA1$^{1-500}$-BARD1$^{1-261}$ with the mixture of D-loop, dsDNA and ssDNA. **d,** DNA binding test of BRCA1$^{1-500}$-BARD1$^{\Delta 163-261}$ with the mixture of D-loop, dsDNA and ssDNA. **e,** Comparison of results obtained using 32 nM of BRCA1-BARD1 (from Extended Data Fig. 1g), BRCA1$^{1-500}$-BARD1 (from Extended Data Fig. 10a), BRCA1$^{1-500}$-BARD1$^{1-261}$ (from **c**) and BRCA1$^{1-500}$-BARD1$^{\Delta 163-261}$ (from **d**). Data are means ± s.d., n=3 or 4. **, P<0.01. **f,** SDS-PAGE of purified BARD1$^{124-270}$. **g,** EMSA to test BARD1$^{124-270}$ for binding the D-loop, DNA bubble (Bubble), double-stranded DNA (dsDNA) and single-stranded DNA (ssDNA). **h,** Nucleoprotein complex consisting of BARD1$^{124-270}$ (16 nM) and radiolabeled D-loop (10 nM) was challenged with an increasing concentration of unlabeled ssDNA, dsDNA, fork, DNA bubble (Bubble) or Dloop as indicated. **i**, Quantification of **h**. Data are means ± s.d., n=3 or 4.

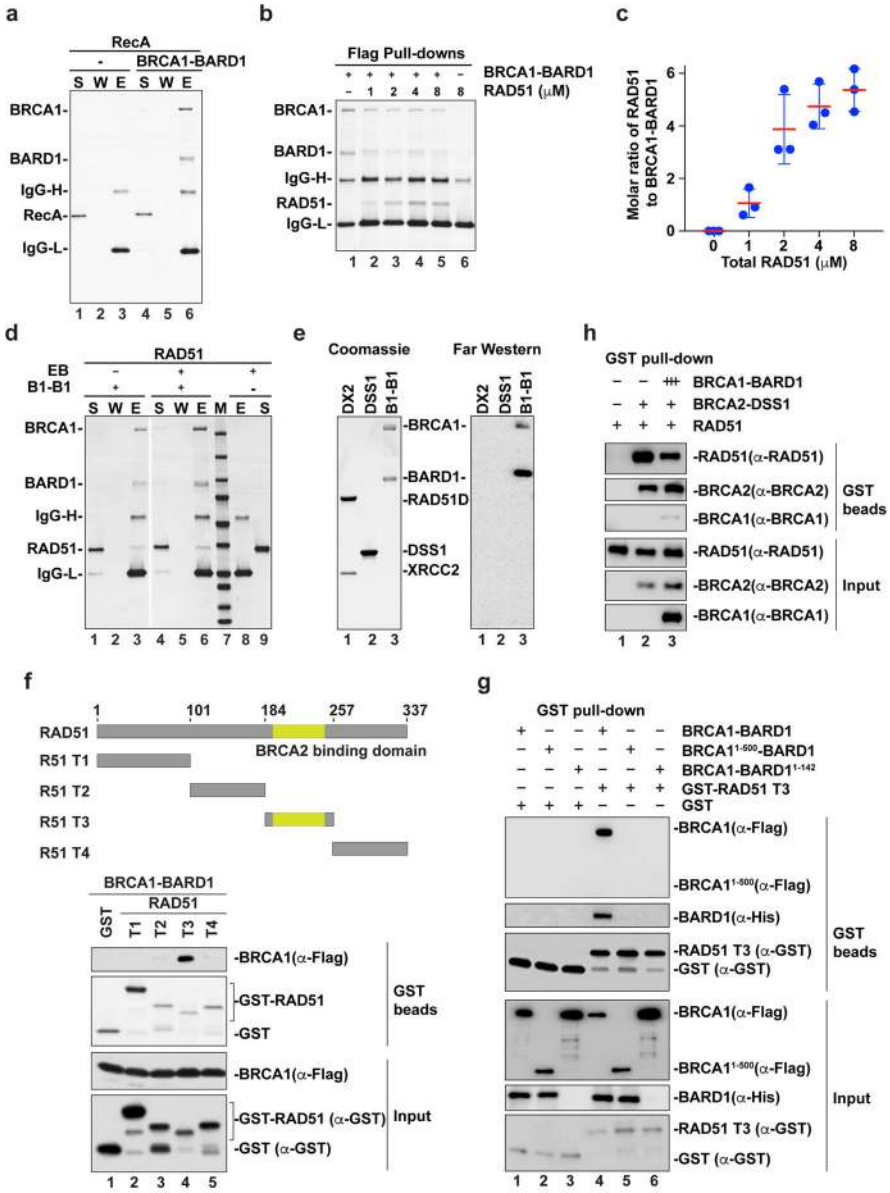

Extended Data Fig. 3. The RAD51 interaction attributes of BRCA1-BARD1

a, Affinity pulldown to test for the interaction of RecA with BRCA1-BARD1 (B1-B1) via the Flag tag on BRCA1. The supernatant (S), wash (W) and eluate (E) fractions were analyzed by SDS-PAGE and Coomassie blue staining. **b,** Affinity pulldown with Flag-tagged BRCA1-BARD1 (66 nM) and an increasing concentration of RAD51 (1, 2, 4 and 8 μM). The eluates from the pulldown experiment were analyzed by SDS-PAGE with Coomassie blue staining. **c,** The amount of BRCA1-BARD1 and RAD51 in lanes 2 to 5 of (**b**) was quantified against known quantities of these protein species run and stained in the same SDS polyacrylamide gel. Data are means ± s.d., n=3. **d,** Affinity pulldown to test for the interaction of RAD51 with BRCA1-BARD1 (B1-B1) with or without ethidium bromide (EB) being present. See (**a**) for definition of symbols. **e,** Far Western analysis to examine RAD51D-XRCC2 (DX2), GST-DSS1 (DSS1) and BRCA1-BARD1 (B1-B1) for RAD51

interaction. **f,** Schematic of the GST-tagged RAD51 fragments examined (upper panel). Results from the pulldown experiment to test for interaction of BRCA1-BARD1 with the RAD51 fragments via the GST tag on the latter (lower panel). RAD51 fragments and BRCA1 were revealed by immunoblot analysis using anti-GST or anti-Flag antibody, respectively. **g,** GST pulldown assay to test for the interaction of the RAD51-T3 fragment with BRCA1-BARD1, BRCA1$^{1-500}$-BARD1 and BRCA1-BARD1$^{1-142}$. The RAD51 fragment, GST, BRCA1 and BARD1 were revealed by immunoblot analysis using anti-GST, anti-Flag or anti-His antibody, respectively. **h,** GST pulldown assay to test for competition between BRCA1-BARD1 (198 nM) and BRCA2-DSS1 (66 nM) for RAD51 (1 μM); DSS1 was GST-tagged. RAD51, BRCA1 and BRCA2 were revealed by immunoblot analysis using antibodies specific for them.

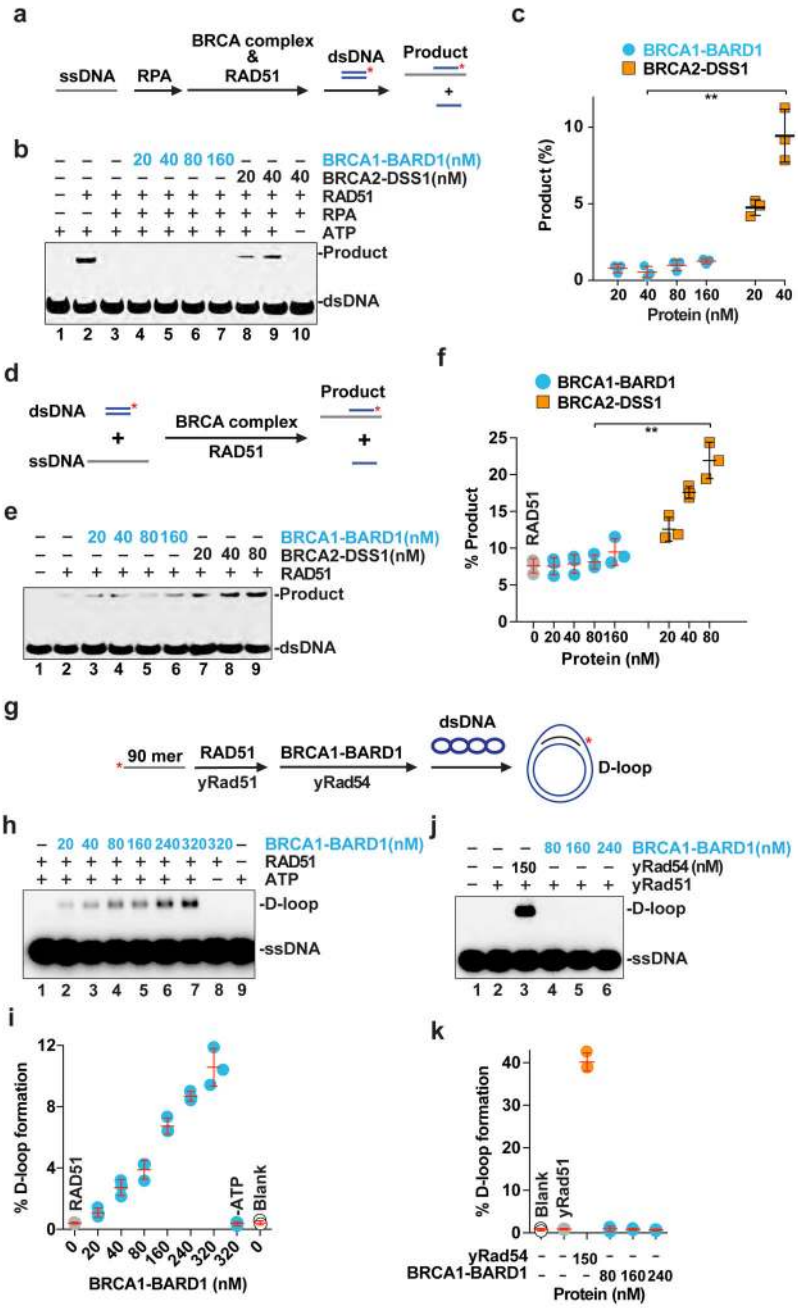

Extended Data Fig. 4. Lack of recombination mediator activity in BRCA1-BARD1 and species-specific enhancement of RAD51 recombinase by BRCA1-BARD1

a, Schematic of the test for mediator activity of BRCA complex (BRCA1-BARD1 and BRCA2-DSS1). **b**, BRCA1-BARD1 and BRCA2-DSS1 were tested for recombination mediator activity with RPA-coated ssDNA as substrate. **c**, Quantification of **b**. Data are means ± s.d., n=3. **d,** Schematic of the test for ssDNA targeting activity of BRCA complex (BRCA1-BARD1 and BRCA2-DSS1). **e**, BRCA1-BARD1 was tested alongside BRCA2-DSS1 for the ability to target RAD51 to ssDNA. **f**, Quantification of **e**. Data are means ± s.d., n=3. **g**. Schematic of the D-loop assay. **h**, D-loop reactions were carried out with the

indicated concentration of BRCA1-BARD1 and ATP as the nucleotide cofactor. **i**, Quantification of **h**. Data are means ± s.d., n=3. **j**, BRCA1-BARD1 and *S. cerevisiae* Rad54 (yRad54) were tested for their influence on D-loop formation catalyzed by *S. cerevisiae* Rad51 (yRad51). **k**, Quantification of **j**. Data are means ± s.d., n=3.

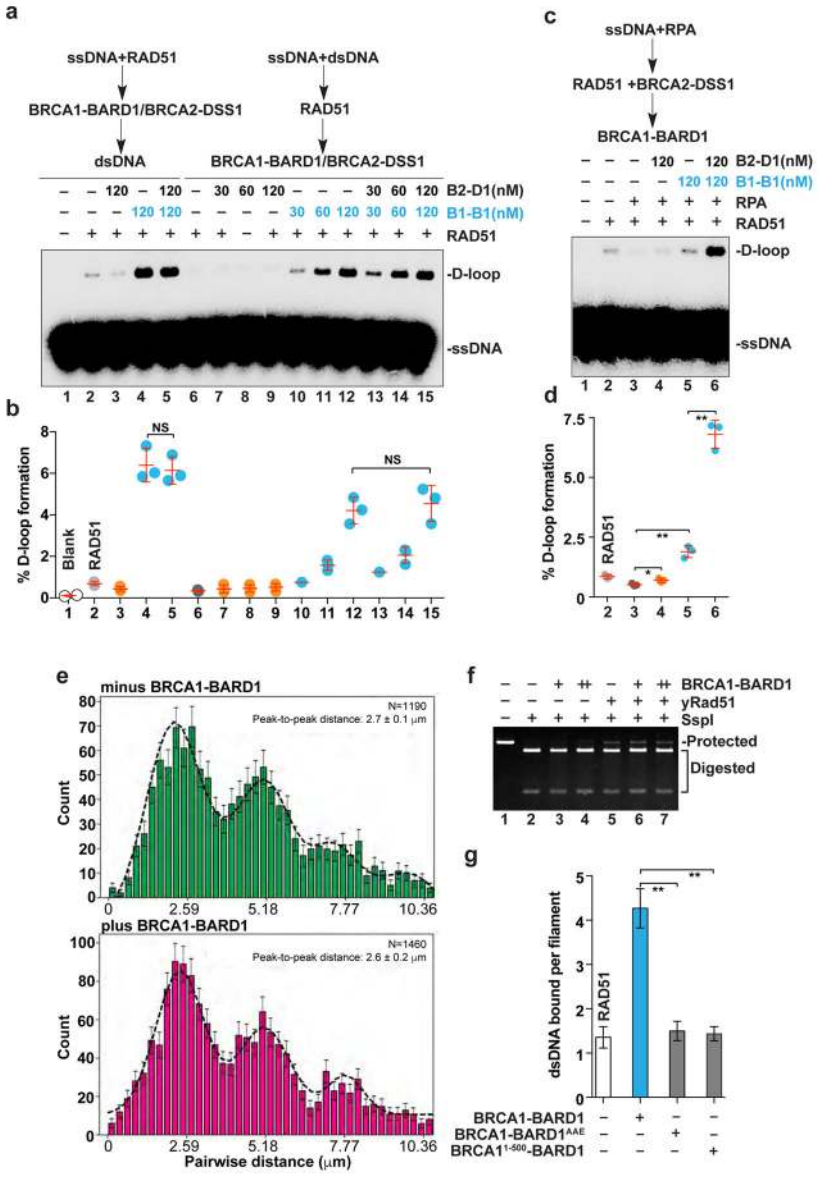

Extended Data Fig. 5. Interplay between BRCA2-DSS1 and BRCA1-BARD1

a, Dloop reactions performed with the indicated concentration of BRCA1-BARD1 (B1-B1), BRCA2-DSS1 (B2-D1), and order of addition of reaction components. **b**, Quantification of **a**. Data are means ± s.d., n=3. NS=non-significant. **c**, D-loop reactions performed with the indicated concentration of BRCA1-BARD1 (B1-B1), BRCA2-DSS1 (B2-D1), and order of addition of reaction components. **d**, Quantification of **c**. Data are means ± s.d., n=3. *, P<0.05; **, P<0.01. **e**, Pairwise distance distributions[39] for Atto565-dsDNA bound to the RAD51-ssDNA filaments with or without BRCA1-BARD1. Data are means ± errors

(determined by bootstrapping). **f,** BRCA1-BARD1 (100 and 200 nM) were tested with filaments of yRad51-ssDNA in synaptic complex assembly as assayed by protection against restriction digest. **g**, Number of dsDNA oligonucleotides bound by the RAD51-ssDNA filament with BRCA1-BARD1, BRCA1-BARD1^{AAE} and BRCA1$^{1-500}$-BARD1. Data are means ± 95% confidence intervals, n=49,54,50,50. **, P<0.01.

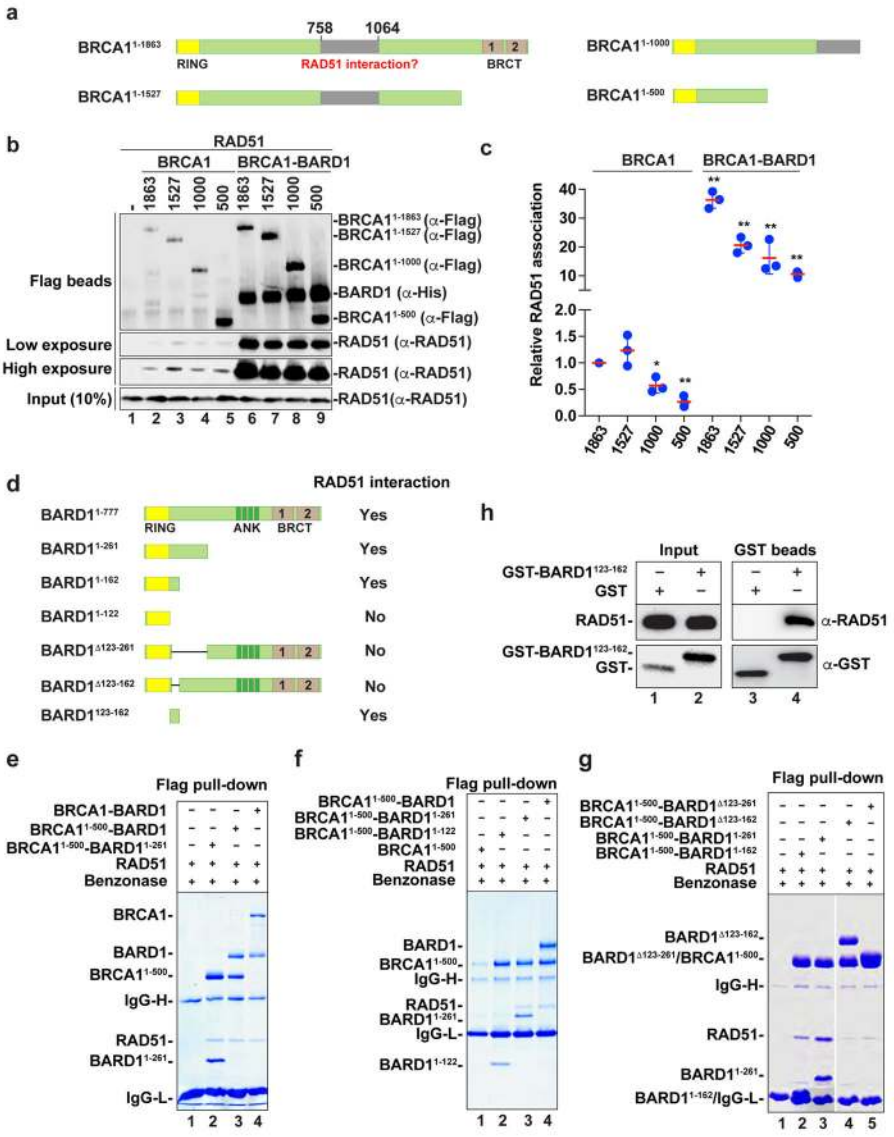

Extended Data Fig. 6. Identification of the RAD51 interaction domain in BRCA1-BARD1

a, Schematic of the BRCA1 deletion variants[37] examined in this study. **b**, Testing BRCA1 deletion variants alone or in complex with BARD1 for the ability to co-immunoprecipitate RAD51 from insect cell extracts using anti-Flag resin with Benzonase treatment. The immunoprecipitates were analyzed by Western blotting with antibodies against the Flag epitope (for BRCA1), the His_6 epitope (for BARD1), or RAD51, as indicated. The cell extracts (10% of total) were probed for their RAD51 content. **c**, Quantification of **b.** Data are means ± s.d., n=3. *, P < 0.05; **, P<0.01. **d**, Summary of the RAD51 interaction ability of

BARD1 truncation mutants, based on the pulldown analyses in **e** (for BRCA1-BARD1, BRCA1$^{1\text{-}500}$-BARD1 and BRCA1$^{1\text{-}500}$-BARD1$^{1\text{-}261}$), **f** (for BRCA1$^{1\text{-}500}$-BARD1, BRCA1$^{1\text{-}500}$-BARD1$^{1\text{-}261}$ and BRCA1$^{1\text{-}500}$-BARD1$^{1\text{-}122}$), **g** (for BRCA1$^{1\text{-}500}$-BARD1$^{\Delta 123\text{-}261}$, BRCA1$^{1\text{-}500}$-BARD1$^{\Delta 123\text{-}162}$, BRCA1$^{1\text{-}500}$-BARD1$^{1\text{-}261}$ and BRCA1$^{1\text{-}500}$-BARD1$^{1\text{-}162}$) and **h** (for BARD1$^{123\text{-}162}$). In **e, f** and **g**, the eluates from the affinity resin were analyzed by SDS-PAGE and Coomassie blue staining. In **h,** the interaction between RAD51 and GST-BARD1$^{123\text{-}162}$ was tested by pulldown using Glutathione resin. The input and eluate fractions were analyzed by Western blotting with antibodies against GST or RAD51, as indicated.

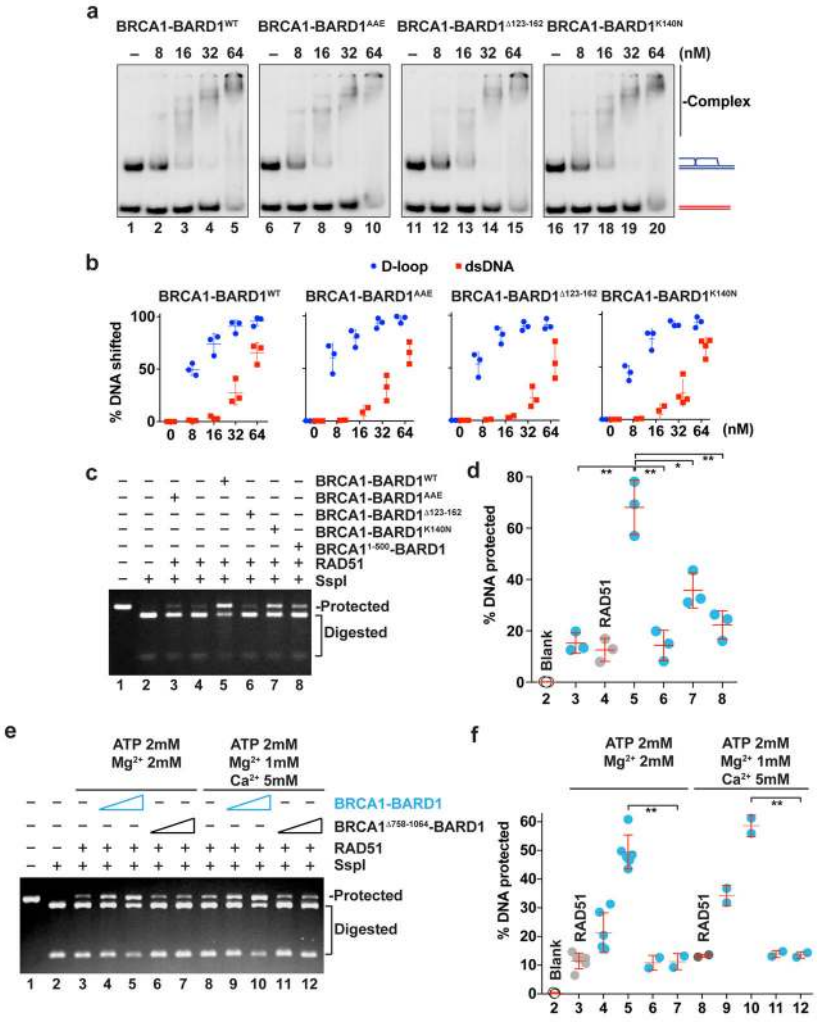

Extended Data Fig. 7. Characterization of BRCA1-BARD1 mutants

a, BRCA1-BARD1, BRCA1-BARD1^{AAE}, BRCA1-BARD1$^{\Delta 123\text{-}162}$, and BRCA1-BARD1^{K140N} were tested for their DNA binding activity using a mixture of radiolabeled D-loop and dsDNA as substrates. **b**, Quantification of **a**. Data are means ± s.d., n=3 or 4. **c**, Wild type and mutant variants of BRCA1-BARD1 (300 nM each) were tested for the ability to promote synaptic complex formation. **d**, Quantification of **c**. Data are means ± s.d., n=3. **e**, Synaptic complex formation by RAD51-ssDNA filament with BRCA1-BARD1 (100 and

200 nM) and BRCA1$^{\Delta 758\text{-}1064}$-BARD1 (100 and 200 nM). **f**, Quantification of **e**. Data are means ± s.d., n=2 or 6. *, P<0.05; **, P<0.01.

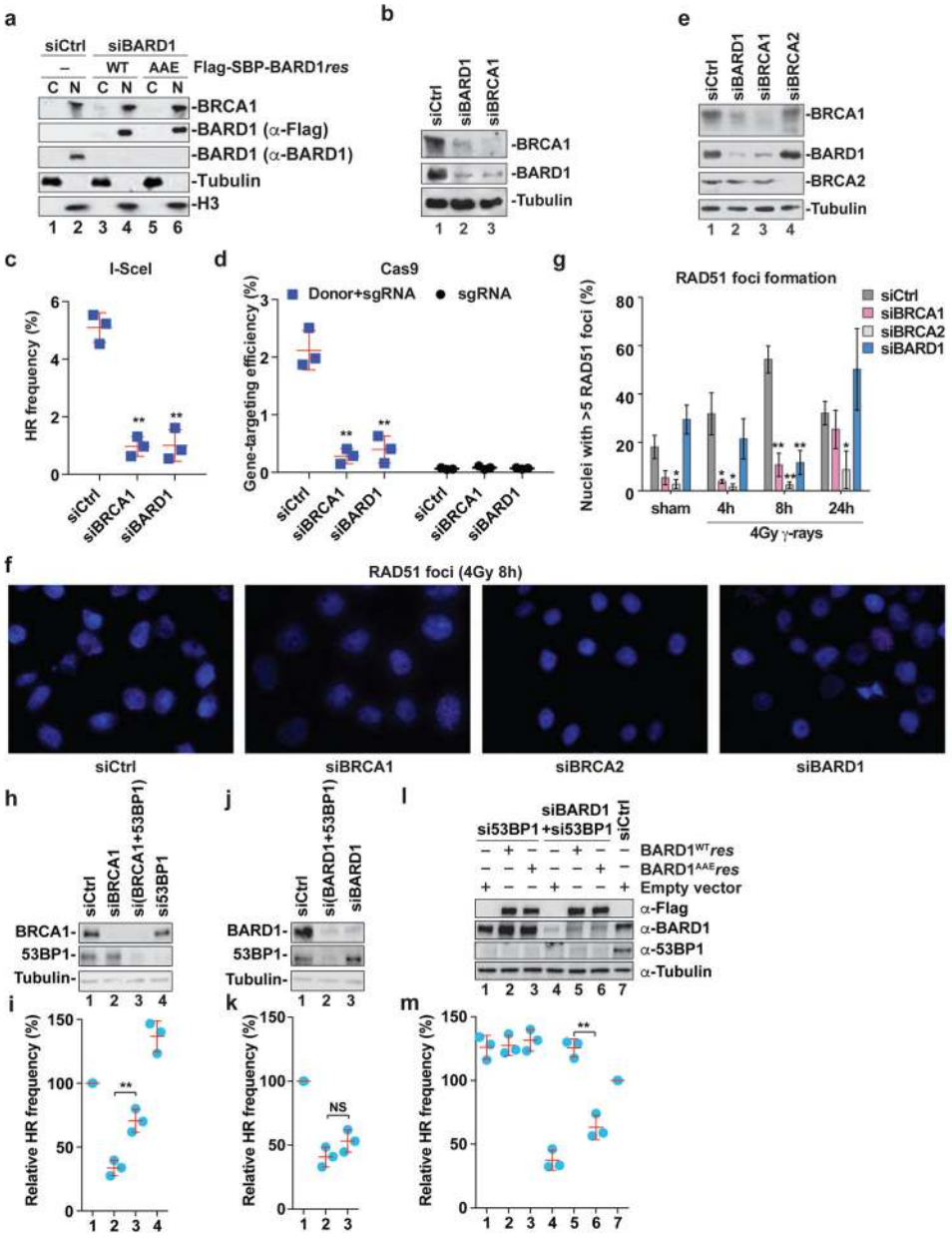

Extended Data Fig. 8. Role of BRCA1 and BARD1 in HR and RAD51 focus formation

a, Western blot to verify the nuclear localization of endogenous BRCA1 and ectopically expressed Flag-SBP tagged BARD1 or the AAE mutant in HeLa cells. The cytoplasmic (C) and nuclear (N) fractions were analyzed for their alpha-Tubulin and histone H3 contents as well. **b**, Western blot analysis to detect endogenous BRCA1 and BARD1 after treatment of DR-U2OS cells with BRCA1 or BARD1 siRNA. **c**, HR frequency in DR-U2OS cells with siRNA-mediated knockdown of BRCA1 or BARD1. Data are means ± s.d., n=3. **d**, Gene-targeting efficiency by CRISPR-CAS9 in U2OS cells with siRNA-mediated knockdown of

BRCA1 or BARD1. Data are means ± s.d., n=3. **e**, Western blot analysis to detect endogenous BRCA1, BARD1 and BRCA2 after treatment of HeLa cells with siRNA against BRCA1, BARD1 or BRCA2 siRNA. Alpha-Tubulin serves as loading control. **f,** Representative micrographs of RAD51 foci (red) in the nuclei of HeLa cells treated with BRCA1, BARD1, BRCA2 or control siRNA 8 h after exposure to 4 Gy γ-rays. Blue: DAPI. **g,** Quantification of RAD51 foci at various time points after exposure to 4 Gy γ-rays or sham irradiation. The mean values ± SEM of 3 or 7 independent experiments are shown. **h**, Western blot analysis to detect endogenous BRCA1 and 53BP1 after treatment of DR-U2OS cells with BRCA1 or 53BP1 siRNA. **i**, HR frequency in DR-U2OS cells with siRNA-mediated knockdown of BRCA1 and/or 53BP1. Data are means ± s.d., n=3. **j**, Western blot analysis to detect endogenous BARD1 and 53BP1 after treatment of DR-U2OS cells with BARD1 and/or 53BP1 siRNA. **k**, HR frequency in DR-U2OS cells with siRNA-mediated knockdown of BARD1 or 53BP1. Data are means ± s.d., n=3. **l**, Western blot analysis to detect ectopically expressed and endogenous BARD1 after treatment of U2OS cells with BARD1 and/or 53BP1 siRNA. As the abundance of ectopically expressed Flag-SBP tagged wild type and mutant BARD1 was lower than endogenous BARD1, we revealed it with anti-Flag antibody in Western blot analysis. **m**, HR frequency in DR-U2OS cells treated with siRNA against BARD1 and/or 53BP1 and stably expressing $BARD1^{WT}$*res* or $BARD1^{AAE}$*res*. Data are means ± s.d., n=3. *, P<0.05; **, P<0.01; NS=non-significant.

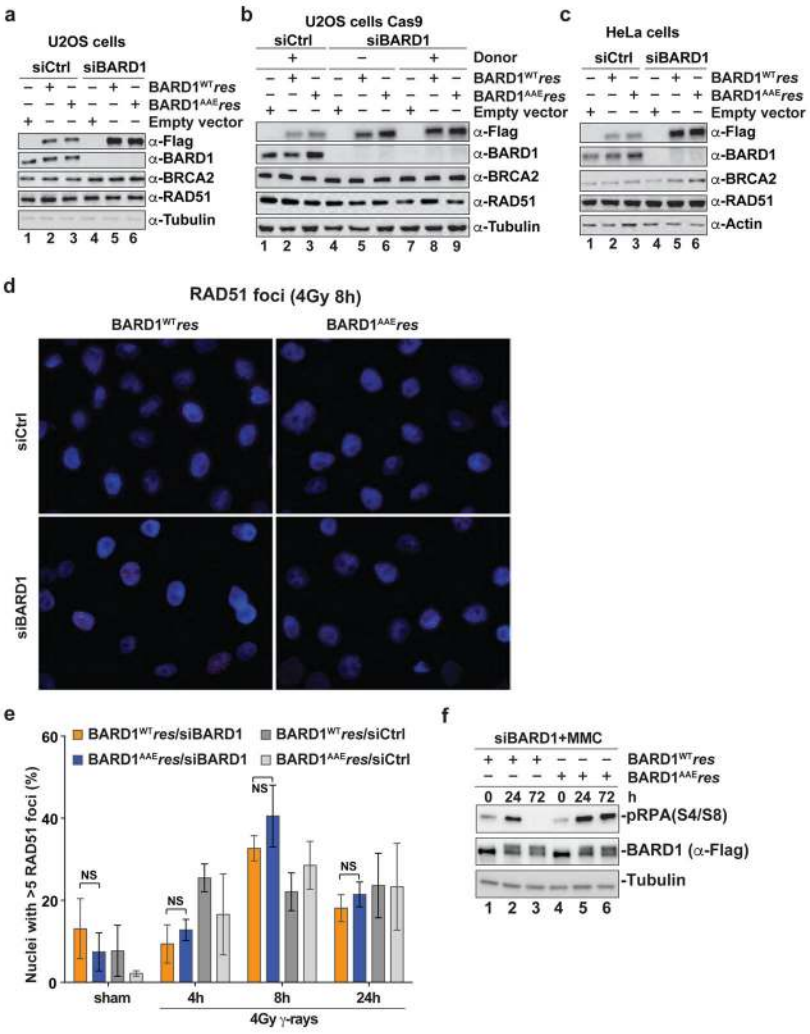

Extended Data Fig. 9. Characterization of human cells expressing BARD1 mutants

a, Western blot analysis to detect ectopically expressed and endogenous BARD1 after treatment of U2OS cells with BARD1 or control siRNA for the experiments in Figure 5b. **b**, Western blot analysis to detect ectopically expressed and endogenous BARD1 after treatment of U2OS cells with BARD1 or control siRNA for the experiments in Figure 5c. **c**, Western blot analysis to detect ectopically expressed and endogenous BARD1 after treatment of HeLa cells with BARD1 or control siRNA for the experiments in Figure 5d. In **a**, **b** and **c**, as the abundance of ectopically expressed Flag-SBP tagged wild type and mutant BARD1 was lower than endogenous BARD1, we revealed it with anti-Flag antibody in Western blot analysis**. d**, Representative micrographs of RAD51 foci (red) in the nuclei of HeLa cells expressing Flag-SBP tagged BARD1^{WT}*res* or BARD1^{AAE}*res* 8 h after exposure to 4 Gy γ-rays. Blue: DAPI. **e**, Quantification of RAD51 foci at various time points after exposure to 4 Gy γ-rays or sham irradiation. The mean values ± SEM of at 3 or 4 independent experiments are shown. NS=non-significant. **f**, Western blot to reveal pRPA32(S4/S8) (with Tubulin as the loading control) at various time points (0, 24 and 72h) after a 1-h treatment with 2 μM MMC.

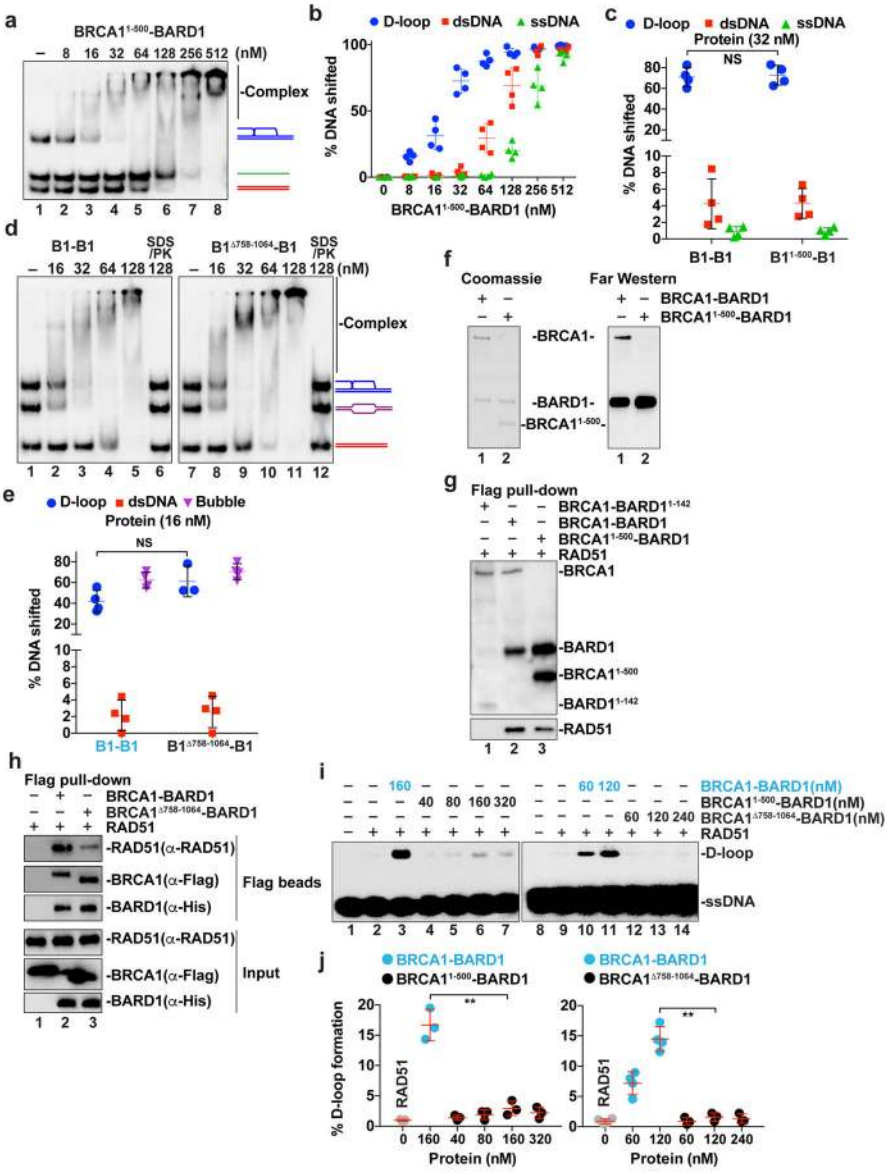

Extended Data Fig. 10. Characterization of BRCA1$^{1\text{-}500}$-BARD1 and BRCA1$^{\Delta 758\text{-}1064}$-BARD1

a, BRCA1$^{1\text{-}500}$-BARD1 was tested for DNA binding using a mixture of radiolabeled D-loop, dsDNA, and ssDNA as substrates. **b**, Quantification of **a**. Data are means ± s.d., n=4. **c**, Comparison of results obtained using 32 nM of BRCA1-BARD1 (from Extended Data Fig. 1g) and BRCA1$^{1\text{-}500}$-BARD1 (from **a**). Data are means ± s.d., n=3. NS=non-significant. **d**, BRCA1-BARD1 and BRCA1$^{\Delta 758\text{-}1064}$-BARD1 was tested for DNA binding using a mixture of radiolabeled D-loop, bubble, and dsDNA as substrates. **e**, Comparison of results obtained using 16 nM of BRCA1-BARD1 and BRCA1$^{\Delta 758\text{-}1064}$-BARD1. Data are means ± s.d., n=4. NS=non-significant. **f**, Far Western analysis to detect RAD51 association with BRCA1$^{1\text{-}500}$ and BARD1 immobilized on nitrocellulose membrane. **g,** Pulldown assay to test for the interaction of RAD51 with BRCA1$^{1\text{-}500}$-BARD1, BRCA1-BARD1$^{1\text{-}142}$ and BRCA1-BARD1 via the Flag tag on the BRCA1 species. The eluates from the various anti-Flag resin

fractions were subjected to immunoblot analysis with anti-Flag (for BRCA1), anti-His (for BARD1) and anti-RAD51 antibodies. **h**, Pulldown assay to test for the interaction between RAD51 and BRCA1-BARD1 or BRCA1$^{\Delta 758\text{-}1064}$-BARD1 via the Flag tag on the BRCA1 species. **i**, BRCA1$^{1\text{-}500}$-BARD1 and BRCA1$^{\Delta 758\text{-}1064}$-BARD1 were tested along with the wild type complex for the ability to enhance RAD51-mediated D-loop formation. **j**, Quantification of **i**. Data are means ± s.d., n=3 or 4. **, P<0.01.

Extended Data Table 1

Oligonucleotides and siRNA used in this study.

Oligo 1	GATGATAATATGGCCACAACCAGCGGCCGCGACTCTAGATC
Oligo 2	GATCTAGAGTCGCGGCCGCTGGTTGTGGCCATATTATCATC
Oligo 3	GAAAGTCAGATATGTTGTGAGCAAGGCAAGTGTCCAGACCCAGCCTGCAATAAAAA
Oligo 4	TTTTTATTGCAGGCTGGGTCTGGACACTTGCCTTGCTCACAACATATCTGACTTTC
Oligo 5	CATTGCATATTTAAAACATGTTGGAAGGCTCGATGCATGCTGATAGCCTACTAGTGCTGCTGGCTTTCAAATGACCTCTTATCAA
Oligo 6	GTCACTTGATAAGAGGTCATTTGAATTCATGGCTTAGAGCTTAATTGCTGAATCTGGTGCTGGGATCCAACATGTTTTAAATATG
Oligo 7	CTGCTACGATGCTAGTCGTAGCTCGGCAGTCGTAGCAGGTTCCCAGCACCAGATTCAGCAATTAAGCTCTAAGCCATGAA
Oligo 8	GACGCTGCCGAATTCTACCAGTGCCTTGCTAGGACATCTTTGCCCACCTGCAGGTTCACCC
Oligo 9	GGACATCTTTGCCCACCTGCAGGTTCACCC
Oligo 10	TGGGTGAACCTGCAGGTGGGCAAAGATGTCC
Oligo 11	GGGTGAACCTGCAGGTGGGCAAAGATGTCCCAGCAAGGCACTGGTAGAATTCGGCAGCGTC
Oligo 12	TTATATCCTTTACTTTGAATTCTATGTTTAACCTTTTACTTATTTTGTATTAGCCGGATCCTTATTTCAATTATGTTCAT
Oligo 13	ATGAACATAATTGAAATAAGGATCCGGCTAATACAAAATAAGTAAAAGGTTAAACATAGAATTCAAAGTAAAGGATATAA
Oligo 14	TCTTATTTATGTCTCTTTTATTTCATTTCCTATATTTATTCCTATTATGTTTTATTCATTTACTTATTCTTTATGTTCATTTTTTATATCC
Oligo 15	TAATACAAAATAAGTAAATGAATAAACAGAGAAAATAAAG
Oilgo 16	CTTTATTTTCTCTGTTTATTCATTTACTTATTTTGTATTA
Oligo 17	AAATCAATCTAAAGTATATATGAGTAAACTTGGTCTGACAGTTACCAATGCTTAATCAGTGAGGCACCTATCTCAGCGATCTGTC
Oligo 18	AATGTTGAATACTCATACTCTTCCTTTTTCAATATTATTGAAGCATTTATCAGGGTTATT
Oligo 19	CAGAATCAGGGGATAACGCAGGAAAGAACATGTGAGCAAAAGGCCAGCAAAAGGCCAGGA
Oligo 20	Atto565CCGGAGGCCTTAGGCCTTAGGCCTTAGGCCT**TCAGCTGTT**AGCCTTAGCTAGCTAGCTAGCTAGCTAGCT
Oligo 21	AGCTAGCTAGCTAGCTAGCTAAGGCT**AACAGCTGA**AGGCCTAAGGCCTAAGGCCTAAGGCCTCCGG
siControl	UAGCCGGUAGACUUAGGUCUG
siBARD1	AAGAGUAAAGCUUCAGUGCAA
siBRCA1	AAGCUCCUCUCACUCUUCAGU
siBRCA2	UUGGAGGAAUAUCGUAGGUAA

Supplemental file

Refer to Web version on PubMed Central for supplementary material.

Acknowledgments

We are grateful to Xiaochun Yu, Jeffrey Parvin, and Graham Dellaire for providing materials. This work was supported by US National Institutes of Health grants ES007061, CA220123, CA168635, CA92584, ES021454,

CA215990 and R35GM118026. J.B.S. was supported by NIH fellowship (F31CA210663). W.Z. and P.S. were also supported by a Basser Innovation Award of the Basser Center for BRCA at Penn Medicine's Abramson Cancer Center.

References

1. Narod SA, Foulkes WD. BRCA1 and BRCA2: 1994 and beyond. Nat Rev Cancer. 2004; 4:665–676. [PubMed: 15343273]
2. Roy R, Chun J, Powell SN. BRCA1 and BRCA2: different roles in a common pathway of genome protection. Nat Rev Cancer. 2012; 12:68–78.
3. Silver DP, Livingston DM. Mechanisms of BRCA1 tumor suppression. Cancer Discov. 2012; 2:679–684. [PubMed: 22843421]
4. Prakash R, Zhang Y, Feng W, Jasin M. Homologous recombination and human health: the roles of BRCA1, BRCA2, and associated proteins. Cold Spring Harb Perspect Biol. 2015; 7:a016600. [PubMed: 25833843]
5. Sawyer SL, et al. Biallelic mutations in BRCA1 cause a new Fanconi anemia subtype. Cancer Discov. 2015; 5:135–142. [PubMed: 25472942]
6. Futreal PA, et al. BRCA1 mutations in primary breast and ovarian carcinomas. Science. 1994; 266:120–122. [PubMed: 7939630]
7. Godwin AK, et al. A common region of deletion on chromosome 17q in both sporadic and familial epithelial ovarian tumors distal to BRCA1. Am J Hum Genet. 1994; 55:666–677. [PubMed: 7942844]
8. Miki Y, et al. A strong candidate for the breast and ovarian cancer susceptibility gene BRCA1. Science. 1994; 266:66–71. [PubMed: 7545954]
9. Savage KI, et al. Identification of a BRCA1-mRNA splicing complex required for efficient DNA repair and maintenance of genomic stability. Mol Cell. 2014; 54:445–459. [PubMed: 24746700]
10. Kawai S, Amano A. BRCA1 regulates microRNA biogenesis via the DROSHA microprocessor complex. J Cell Biol. 2012; 197:201–208. [PubMed: 22492723]
11. Chang S, Sharan SK. BRCA1 and microRNAs: emerging networks and potential therapeutic targets. Mol Cells. 2012; 34:425–432. [PubMed: 22936386]
12. Kleiman FE, Manley JL. Functional interaction of BRCA1-associated BARD1 with polyadenylation factor CstF-50. Science. 1999; 285:1576–1579. [PubMed: 10477523]
13. Kleiman FE, Manley JL. The BARD1-CstF-50 interaction links mRNA 3′ end formation to DNA damage and tumor suppression. Cell. 2001; 104:743–753. [PubMed: 11257228]
14. Deng CX. BRCA1: cell cycle checkpoint, genetic instability, DNA damage response and cancer evolution. Nucleic Acids Res. 2006; 34:1416–1426. [PubMed: 16522651]
15. Schlacher K, Wu H, Jasin M. A distinct replication fork protection pathway connects Fanconi anemia tumor suppressors to RAD51-BRCA1/2. Cancer Cell. 2012; 22:106–116. [PubMed: 22789542]
16. Hatchi E, et al. BRCA1 recruitment to transcriptional pause sites is required for Rloop-driven DNA damage repair. Mol Cell. 2015; 57:636–647. [PubMed: 25699710]
17. Scully R, et al. Association of BRCA1 with Rad51 in mitotic and meiotic cells. Cell. 1997; 88:265–275. [PubMed: 9008167]
18. Moynahan ME, Chiu JW, Koller BH, Jasin M. Brca1 controls homology-directed DNA repair. Mol Cell. 1999; 4:511–518. [PubMed: 10549283]
19. Caestecker KW, Van de Walle GR. The role of BRCA1 in DNA double-strand repair: past and present. Exp Cell Res. 2013; 319:575–587. [PubMed: 23200932]
20. Wu LC, et al. Identification of a RING protein that can interact in vivo with the BRCA1 gene product. Nat Genet. 1996; 14:430–440. [PubMed: 8944023]
21. Irminger-Finger I, Jefford CE. Is there more to BARD1 than BRCA1? Nat Rev Cancer. 2006; 6:382–391. [PubMed: 16633366]
22. McCarthy EE, Celebi JT, Baer R, Ludwig T. Loss of Bard1, the heterodimeric partner of the Brca1 tumor suppressor, results in early embryonic lethality and chromosomal instability. Mol Cell Biol. 2003; 23:5056–5063. [PubMed: 12832489]

23. Westermark UK, et al. BARD1 participates with BRCA1 in homology-directed repair of chromosome breaks. Mol Cell Biol. 2003; 23:7926–7936. [PubMed: 14560035]
24. Laufer M, et al. Structural requirements for the BARD1 tumor suppressor in chromosomal stability and homology-directed DNA repair. J Biol Chem. 2007; 282:34325–34333. [PubMed: 17848578]
25. Densham RM, et al. Human BRCA1-BARD1 ubiquitin ligase activity counteracts chromatin barriers to DNA resection. Nat Struct Mol Biol. 2016; 23:647–655. [PubMed: 27239795]
26. Thai TH, et al. Mutations in the BRCA1-associated RING domain (BARD1) gene in primary breast, ovarian and uterine cancers. Hum Mol Genet. 1998; 7:195–202. [PubMed: 9425226]
27. Ghimenti C, et al. Germline mutations of the BRCA1-associated ring domain (BARD1) gene in breast and breast/ovarian families negative for BRCA1 and BRCA2 alterations. Genes Chromosomes Cancer. 2002; 33:235–242. [PubMed: 11807980]
28. Ishitobi M, et al. Mutational analysis of BARD1 in familial breast cancer patients in Japan. Cancer Lett. 2003; 200:1–7. [PubMed: 14550946]
29. Karppinen SM, Heikkinen K, Rapakko K, Winqvist R. Mutation screening of the BARD1 gene: evidence for involvement of the Cys557Ser allele in hereditary susceptibility to breast cancer. J Med Genet. 2004; 41:e114. [PubMed: 15342711]
30. Wu JY, et al. Aberrant expression of BARD1 in breast and ovarian cancers with poor prognosis. Int J Cancer. 2006; 118:1215–1226. [PubMed: 16152612]
31. Symington LS. DNA repair: Making the cut. Nature. 2014; 514:39–40. [PubMed: 25231858]
32. San Filippo J, Sung P, Klein H. Mechanism of eukaryotic homologous recombination. Annu Rev Biochem. 2008; 77:229–257. [PubMed: 18275380]
33. Daley JM, Sung P. 53BP1, BRCA1, and the choice between recombination and end joining at DNA double-strand breaks. Mol Cell Biol. 2014; 34:1380–1388. [PubMed: 24469398]
34. Paull TT, Cortez D, Bowers B, Elledge SJ, Gellert M. Direct DNA binding by Brca1. Proc Natl Acad Sci U S A. 2001; 98:6086–6091. [PubMed: 11353843]
35. Simons AM, et al. BRCA1 DNA-binding activity is stimulated by BARD1. Cancer Res. 2006; 66:2012–2018. [PubMed: 16489000]
36. Zhao W, et al. Promotion of BRCA2-Dependent Homologous Recombination by DSS1 via RPA Targeting and DNA Mimicry. Mol Cell. 2015; 59:176–187. [PubMed: 26145171]
37. San Filippo J, et al. Recombination mediator and Rad51 targeting activities of a human BRCA2 polypeptide. J Biol Chem. 2006; 281:11649–11657. [PubMed: 16513631]
38. Jensen RB, Carreira A, Kowalczykowski SC. Purified human BRCA2 stimulates RAD51-mediated recombination. Nature. 2010; 467:678–683. [PubMed: 20729832]
39. Qi Z, et al. DNA sequence alignment by microhomology sampling during homologous recombination. Cell. 2015; 160:856–869. [PubMed: 25684365]
40. Lee JY, et al. DNA RECOMBINATION. Base triplet stepping by the Rad51/RecA family of recombinases. Science. 2015; 349:977–981. [PubMed: 26315438]
41. Pellegrini L, et al. Insights into DNA recombination from the structure of a RAD51-BRCA2 complex. Nature. 2002; 420:287–293. [PubMed: 12442171]
42. Zhao W, Sung P. Significance of ligand interactions involving Hop2-Mnd1 and the RAD51 and DMC1 recombinases in homologous DNA repair and XX ovarian dysgenesis. Nucleic Acids Res. 2015; 43:4055–4066. [PubMed: 25820426]
43. Kovalenko OV, Wiese C, Schild D. RAD51AP2, a novel vertebrate- and meiotic-specific protein, shares a conserved RAD51-interacting C-terminal domain with RAD51AP1/PIR51. Nucleic Acids Res. 2006; 34:5081–5092. [PubMed: 16990250]
44. Cerami E, et al. The cBio cancer genomics portal: an open platform for exploring multidimensional cancer genomics data. Cancer Discov. 2012; 2:401–404. [PubMed: 22588877]
45. Gao J, et al. Integrative analysis of complex cancer genomics and clinical profiles using the cBioPortal. Sci Signal. 2013; 6:pl1. [PubMed: 23550210]
46. Nakanishi K, et al. Human Fanconi anemia monoubiquitination pathway promotes homologous DNA repair. Proc Natl Acad Sci U S A. 2005; 102:1110–1115. [PubMed: 15650050]
47. Xia B, et al. Control of BRCA2 cellular and clinical functions by a nuclear partner, PALB2. Mol Cell. 2006; 22:719–729. [PubMed: 16793542]

48. Pinder J, Salsman J, Dellaire G. Nuclear domain 'knock-in' screen for the evaluation and identification of small molecule enhancers of CRISPR-based genome editing. Nucleic Acids Res. 2015; 43:9379–9392. [PubMed: 26429972]

49. Orthwein A, et al. A mechanism for the suppression of homologous recombination in G1 cells. Nature. 2015; 528:422–426. [PubMed: 26649820]

50. Bunting SF, et al. 53BP1 inhibits homologous recombination in brca1-deficient cells by blocking resection of DNA breaks. Cell. 2010; 141:243–254. [PubMed: 20362325]

51. Sigurdsson S, Trujillo K, Song B, Stratton S, Sung P. Basis for avid homologous DNA strand exchange by human Rad51 and RPA. J Biol Chem. 2001; 276:8798–8806. [PubMed: 11124265]

52. Sung P. Catalysis of ATP-dependent homologous DNA pairing and strand exchange by yeast RAD51 protein. Science. 1994; 265:1241–1243. [PubMed: 8066464]

53. Zhao W, et al. Mechanistic insights into the role of Hop2-Mnd1 in meiotic homologous DNA pairing. Nucleic Acids Res. 2014; 42:906–917. [PubMed: 24150939]

54. Wiese C, et al. Promotion of homologous recombination and genomic stability by RAD51AP1 via RAD51 recombinase enhancement. Mol Cell. 2007; 28:482–490. [PubMed: 17996711]

55. Dignam JD, Lebovitz RM, Roeder RG. Accurate transcription initiation by RNA polymerase II in a soluble extract from isolated mammalian nuclei. Nucleic Acids Res. 1983; 11:1475–1489. [PubMed: 6828386]

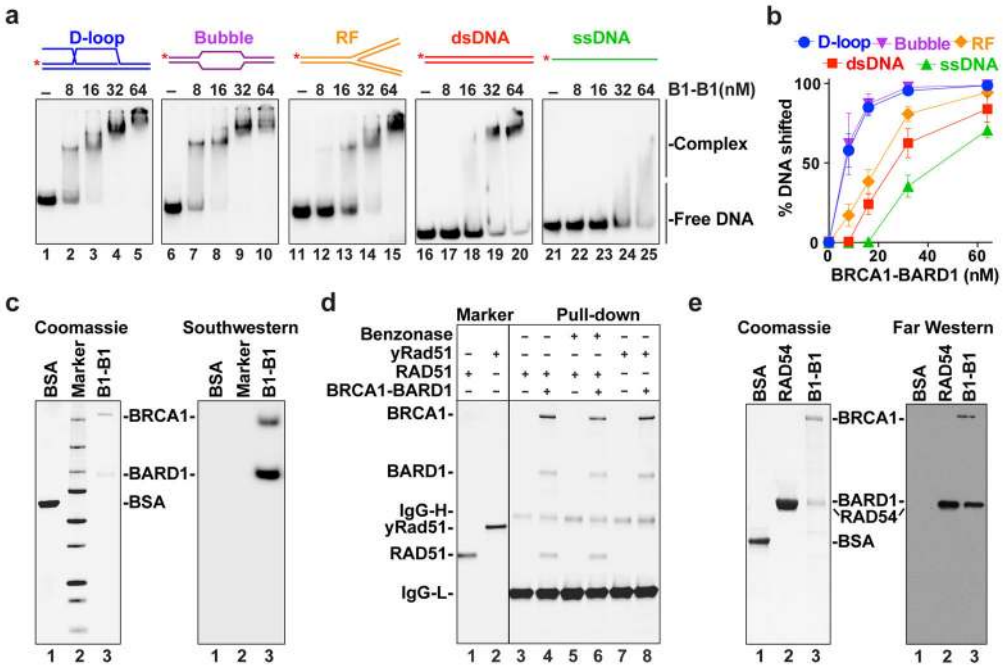

Fig. 1. DNA binding and RAD51 interaction attributes of BRCA1-BARD1

a, Binding of D-loop, DNA bubble (Bubble), replication fork (RF), dsDNA and ssDNA. **b**, Quantification of **a**. Data are means ± s.d., n=3 or 5. **c**, Southwestern analysis to test Dloop binding. BSA was the negative control. **d**, Pulldown analysis for interaction of RAD51 or yRad51 with BRCA1-BARD1. **e**, Far Western analysis for interaction of BRCA1 and BARD1 with RAD51. B1-B1, BRCA1-BARD1. BSA and RAD54 were the negative and positive controls, respectively.

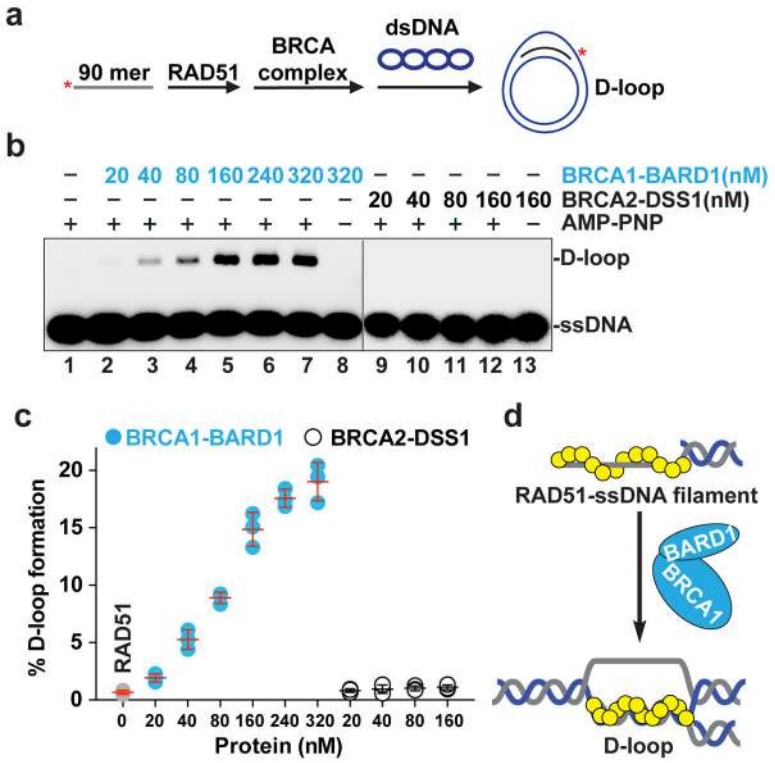

Fig. 2. Enhancement of RAD51-mediated D-loop formation by BRCA1-BARD1

a, Assay schematic. **b,** Reactions with BRCA1-BARD1 and BRCA2-DSS1. **c**, Quantification of **b**. Data are means ± s.d., n=3. **d**, Cartoon depicting the role of BRCA1-BARD1 in DNA strand invasion.

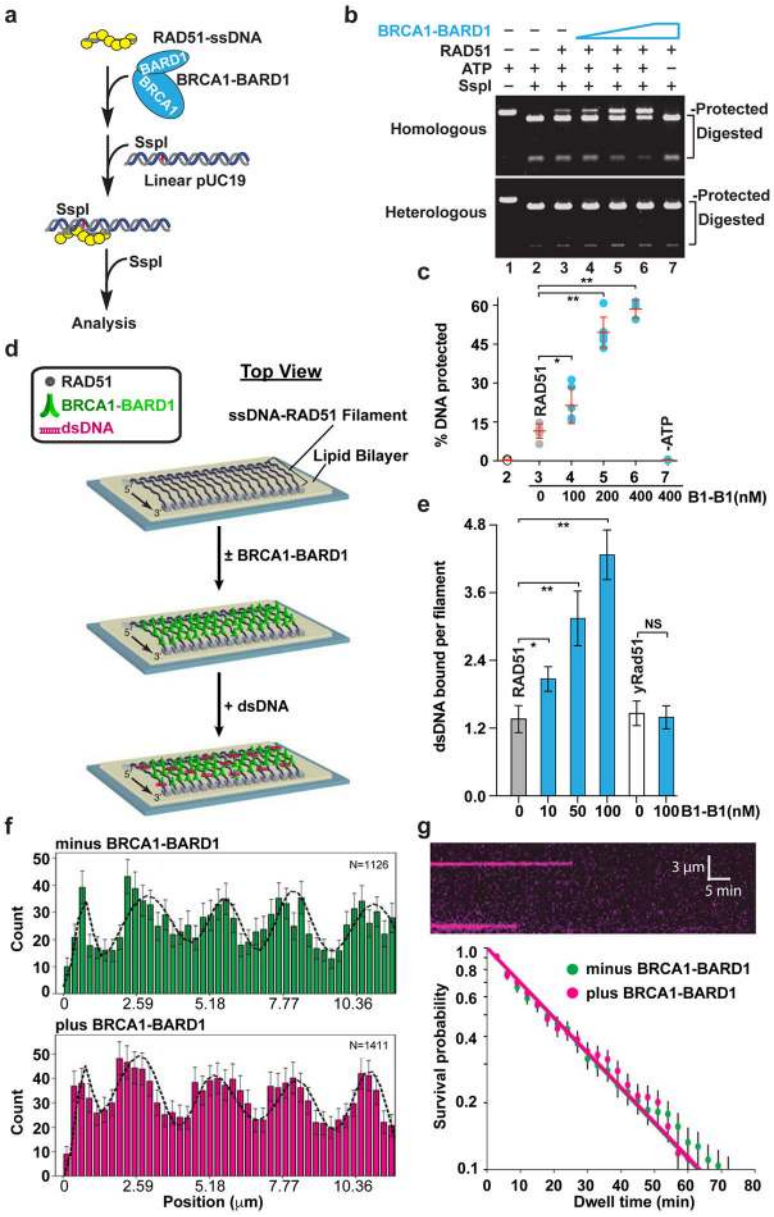

Fig. 3. Promotion of synaptic complex formation by BRCA1-BARD1

a, Synaptic complex assay schematic. **b**, Synaptic complex formation by the RAD51-ssDNA filament and BRCA1-BARD1. **c**, Quantification of **b**. Data are means ± s.d., n=3 or 6. **d,** DNA curtain assay schematic[39,40]. **e,** Number of dsDNA oligonucleotides bound by each RAD51-ssDNA or yRad51-ssDNA filament as a function of BRCA1-BARD1 concentration. Data are means ± 95% confidence intervals, n=49, 50, 38, 54, 51 or 53. **f**, Binding distribution for Atto565-dsDNA with or without BRCA1-BARD1. **g,** Semi-log survival plot of the synaptic complex with and without 100 nM BRCA1-BARD1. *, P<0.05; **, P<0.01. NS=non-significant. In f and g, data are means ± errors (determined by bootstrapping). The multiguassian in f and the lines in g were fitted with least squares analysis.

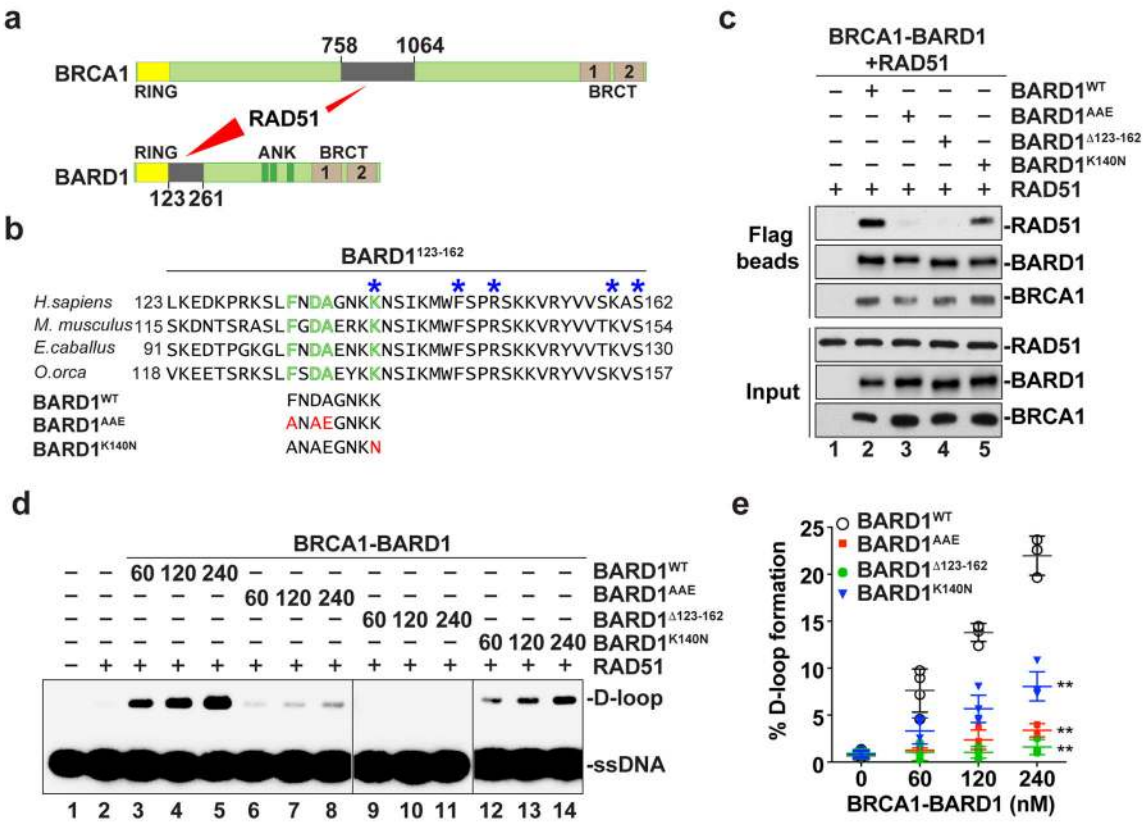

Fig. 4. Relevance of the BARD1-RAD51 complex in DNA strand invasion

a, Domains in BRCA1-BARD1. **b,** Alignment of the RAD51 interaction domain in BARD1 orthologs. The highlighted residues (in green) were changed to AAE or N (in red). The asterisks denote BARD1 mutations found in human cancers (cBioPortal for Cancer Genomic). **c**, Testing of RAD51 interaction with wild type or mutant BRCA1-BARD1. **d**, Examination of BRCA1-BARD1 mutants in the D-loop reaction. **e**, Quantification of **d**. Data are means ± s.d., n=3, 4 or 5. P values were calculated using two-way ANOVA and multiple comparisons were corrected by the Bonferroni method. **, P<0.01.

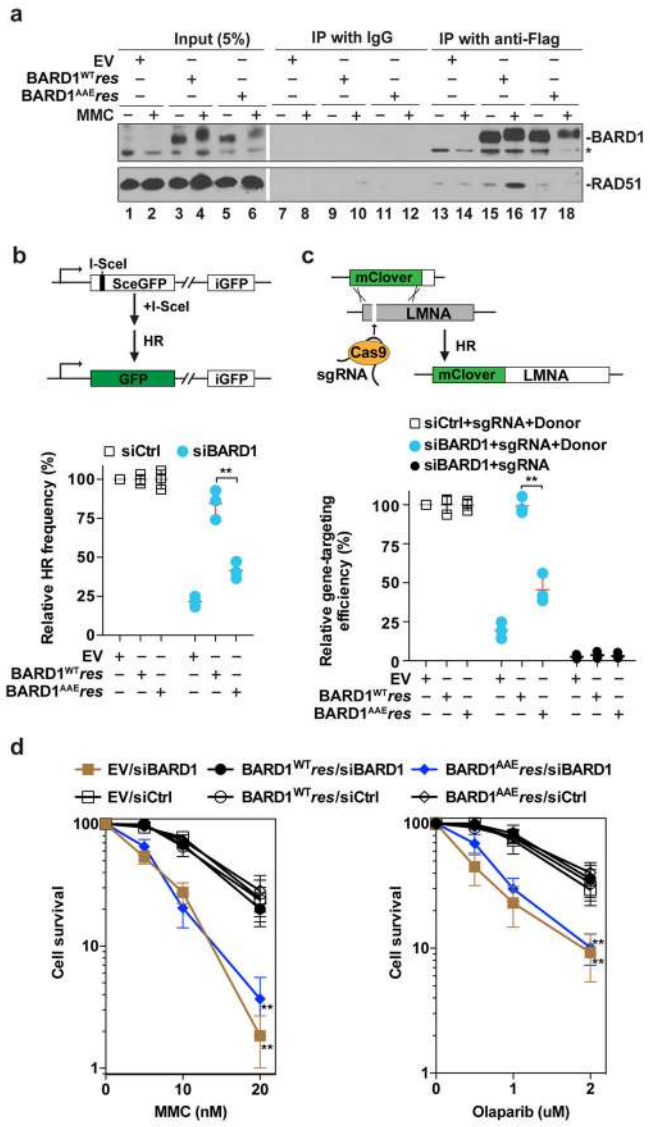

Fig. 5. Biological relevance of the BARD1-RAD51 complex

a, Immunoprecipitation to test BARD1^{WT} and BARD1^{AAE} for RAD51 association upon MMC treatment. The asterisk denotes a non-specific band. **b**, Schematic of the DR-GFP reporter assay (upper). Results obtained with cells expressing BARD1^{WT}*res* or BARD1^{AAE}*res* upon treatment with BARD1 siRNA or control siRNA (siCtrl) (bottom). Data are means ± s.d., n=3. **c**, Schematic of the CRISPR/Cas9 gene targeting assay (upper). Results obtained with cells expressing BARD1^{WT}*res* or BARD1^{AAE}*res* upon treatment with BARD1 siRNA or siCtrl. Data are means ± s.d., n=3. **d**, Clonogenic survival of cells expressing BARD1^{WT}*res* or BARD1^{AAE}*res* upon Olaparib or MMC treatment. Data are means ± s.d., n=3. EV, empty vector. P values were calculated using two-way ANOVA and multiple comparisons were corrected by the Bonferroni method. **, P<0.01.

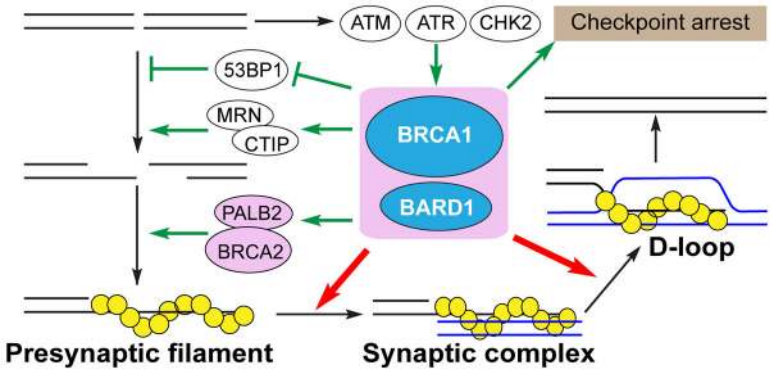

Fig. 6. Model for BRCA1-BARD1 functions

Aside from a co-operative role with PALB2-BRCA2 in RAD51 presynaptic filament assembly (green arrows), our work has revealed a function of BRCA1-BARD1 in the promotion of homologous DNA pairing (red arrows). Previous studies have provided evidence that BRCA1-BARD1 antagonizes 53BP1 in DNA end resection (green blocks) and promotes MRN/CtIP activity (green arrows), and for a role of the complex in cell cycle checkpoint regulation (green arrows).